Physics – Uspekhi **52** (8) 765 – 788 (2009)

REVIEWS OF TOPICAL PROBLEMS PACS numbers: 94.20.Ss, **94.30.–d**, 94.30.Bg, 94.30.Ch

Magnetospheres of planets with an intrinsic magnetic field

E S Belenkaya

DOI: 10.3367/UFNe.0179.200908a.0809

Contents

Abstract. The review presents modern views on the physics of magnetospheres of Solar System planets having an intrinsic magnetic field, and on the structure of magnetospheric magnetic fields. Magnetic fields are generated in the interiors of Mercury, Earth, Jupiter, Saturn, Uranus, and Neptune via the dynamo mechanism. These fields are so strong that they serve as obstacles for the plasma stream of the solar wind. A magnetosphere surrounding a planet forms as the result of interaction between the solar wind and the planetary magnetic field. The dynamics of magnetospheres are primarily enforced by solar wind variations. Each magnetosphere is unique. The review considers common and individual sources of magnetic fields and the properties of planetary magnetospheres.

1. Introduction

Exploration of planetary magnetospheres is a relatively young and rapidly developing area of space research. The main body of information on the magnetospheres of planets of the Solar System has been collected over the last 50 years. It was found that planets having an intrinsic magnetic field — Mercury, the Earth, Jupiter, Saturn, Uranus, and Neptune — are surrounded by magnetospheres. A magnetosphere appears owing to the interaction of the solar wind with the planet magnetic field; the magnetic field prevails inside the magnetosphere, preventing the solar wind from directly penetrating to the planet. The magnetosphere is filled with plasma, fast particles, and emissions of various types.

E S Belenkaya Skobeltsyn Institute of Nuclear Physics, Lomonosov Moscow State University, Vorob'evy gory 1, str. 2, 119992 Moscow, Russian Federation
Tel. (7-495) 939 39 21. Fax (7-495) 939 35 53
E-mail: elena@dec1.sinp.msu.ru

Received 2 February 2009, revised 7 March 2009
Uspekhi Fizicheskikh Nauk **179** (8) 809 – 835 (2009)
DOI: 10.3367/UFNr.0179.200908a.0809
Translated by S V Danilov; edited by A M Semikhatov

The solar wind is a relatively low-density stream of hot, quasineutral, fully ionized hydrogen–helium plasma (composed of protons, neutrons, and α-particles) continuously emitted from the solar corona and accelerated near the Sun to supersonic and super-Alfvén speeds. At the boundary of the heliosphere (at the distance ~ 100 AU), the solar wind interacts with interstellar matter. In the Earth's orbit, the mean speed of the solar wind is 400–500 km s^{-1}, the mean Alfvén speed is 60 km s^{-1}, the ion density is of the order of 5–10 cm^{-3}, and the temperatures of ions and electrons respectively reach 10^5 and 2×10^5 K. The solar wind density decreases as the inverse of the squared distance to the Sun, while its speed stays virtually constant. The plasma of the solar wind carries a large-scale interplanetary magnetic field (IMF) from the Sun to the Solar System periphery. The IMF is formed by the solar magnetic field and the field of the heliospheric current sheet separating zones of oppositely directed magnetic field lines (from and toward the Sun in different solar hemispheres) [1].

The outer boundary of the magnetosphere is called the magnetopause. It is a thin current sheet where the direction and magnitude of the magnetic field change. The supersonic solar wind stream creates an interplanetary bow shock wave on the dayside before the magnetopause. On this wave, the solar wind stream is decelerated, compressed, and heated. The region with turbulent plasma between the bow shock wave and the magnetopause is called the magnetosheath. On the inner side, the magnetosphere is bounded by the ionosphere — the upper layer of the atmosphere (located at altitudes in excess of 60 km from the Earth surface) partly ionized by solar radiation in the far-ultraviolet and X-ray bands. The Earth's ionosphere, like the solar wind, serves as a source of magnetospheric plasma, providing mostly protons, single-charged helium, and oxygen, as well as electrons, which ensure quasineutrality. The cusp is the region near the magnetopause with a minimal magnetic field, filled with a nearly steady dense plasma of the magnetosheath and located on high-latitude magnetic field lines of the magnetosphere.

The solar wind and the interplanetary magnetic field carried by it form an asymmetric magnetosphere, compressed on the dayside and stretching as a long tail on the nightside. The size of the magnetosphere is determined by the balance of the solar wind and magnetospheric magnetic field pressures across their common boundary. The geometry of the magnetic field in the magnetotail is shaped by the transverse current in the neutral current sheet of the tail. This current closes on the magnetopause. Other currents also flow at the magnetopause, which shield the interplanetary space from the magnetic field of magnetospheric sources. The energy transferred from the solar wind to the magnetosphere eventually controls various levels of internal magnetic activity in the magnetosphere. When the level of energy accumulated in the magnetotail exceeds the critical energy, a substorm emerges.

The space plasma is so rarefied that Coulomb interactions between particles are practically absent outside the ionosphere. Correspondingly, a large-scale magnetic field gives rise to the motion of charged particles around field lines along spiral trajectories at the cyclotron frequency, which exceeds the collision frequency. Such a plasma is called magnetized and it is anisotropic because the magnetic field sets a direction. The conductivity along the direction of the magnetic field is so high that the magnetic field lines are frozen in the plasma, i.e., move with it. The high field-aligned conductivity implies large values of the magnetic Reynolds number. As a consequence, the magnetic flux in an arbitrary magnetic field tube is conserved, and the plasma and the magnetic field move as a single entity. The evolution of collective processes in a colissionless plasma is dissimilar to that in a plasma experiencing collisions, and the distribution of particles over velocities can strongly deviate from the Maxwellian one (beams of fast particles, anisotropy of temperatures), which triggers numerous microinstabilities. Therefore, the motion of cosmic plasma is determined not only by the local conditions but also by the state of the plasma and magnetic field in remote regions. Large-scale magnetic and electric fields combine and connect separate objects of the global cosmic system.

Magnetohydrodynamics (MHD), the branch of science dealing with large-scale motions of conducting liquids, gases, and plasmas in a magnetic field, is commonly used to describe processes occurring in a cosmic plasma. The equation for the magnetic field induction vector is [2]

$$\frac{\partial \mathbf{B}}{\partial t} = \nabla \times [\mathbf{V} \times \mathbf{B}] + \eta_{\mathrm{m}} \nabla^2 \mathbf{B}\,, \qquad \eta_{\mathrm{m}} = (\mu_0 \sigma)^{-1}\,, \tag{1}$$

where η_{m} is the magnetic diffusion coefficient, σ is the conductivity, and μ_0 is the magnetic permeability of the vacuum. It was noted in [3] that in many cases, in particular in deriving the induction equation, it suffices to write the specific electric resistivity tensor as $\underline{\eta}_{\mathrm{e}ij} = \eta_{\mathrm{e}} \delta_{ij}$, where η_{e} is the scalar specific electric resistivity, the quantity inverse to the specific electric conductivity σ. The magnetic diffusion coefficient is expressed as $\eta_{\mathrm{m}} = \eta_{\mathrm{e}}/\mu_0$. The first term in the right-hand side of Eqn (1) describes the convection of a magnetic field with the plasma flow, and the second term describes the diffusion of the field in the plasma. In the MHD framework, the absence of dissipation is linked to the preservation of the magnetic field topology [4]. If the first term in Eqn (1) is much larger than the second one, the magnetic flux is frozen in the plasma and the magnetic field topology cannot change. If the second term exceeds the first one, the connection between the magnetic field and plasma becomes weaker and the topology is no longer constrained. The ratio of the first term to the second is characterized by the Lundquist number $S_{\mathrm{L}} = V_{\mathrm{A}} l/\eta_{\mathrm{m}}$ (V_{A} is the Alfvén speed and l is the characteristic size) or the magnetic Reynolds number $R_{\mathrm{m}} = Vl/\eta_{\mathrm{m}}$ (V is the mean flow velocity). Media studied in geo- and astrophysical applications of MHD are characterized by high conductivity and/or large sizes, i.e., S_{L} and $R_{\mathrm{m}} \gg 1$.

Hence, the frozen-in character of the magnetic field corresponds to large values of S_{L} and/or R_{m}. If this character is preserved, i.e., the interaction of the solar wind with a planet remains 'ideal,' then the plasma of the solar wind and the magnetospheric plasma do not mix, but form distinct regions separated by a thin current sheet (magnetopause).

For structures of a small characteristic spatial size or finite conductivity, for example, for some current sheets, the values of S_{L} and/or R_{m} can be less than or of the order of unity. In these regions, called dissipative or diffusive, the leading role is played by the effects of finite electric conductivity, and the freezing-in conditions can be violated. As a consequence, the reconnection of magnetic fields becomes possible.

A distinctive feature of the reconnection process is a change in the topology of the magnetic field in a plasma with a high finite conductivity. The ratio of the volume of a dissipating region to that of the surrounding space tends to zero as η_{m} tends to zero. Nevertheless, the magnetic reconnection occurring in diffusive regions of relatively small volume leads to fundamental changes in the macroscopic topology of global magnetic fields. The reconnection is an essentially nonlocal process manifested on large spatial scales [5].

The reconnection of magnetic field lines in a high-conductivity plasma is accompanied by a rapid release of magnetic energy, its subsequent transformation into the kinetic energy of the plasma, heating, emission and particle acceleration. The magnetic reconnection is characterized by an immense variety of types and manifestations in astrophysical, space, and laboratory plasmas. Similarly to many fundamental notions in physics, the reconnection combines a broad set of phenomena within a single universal law [3, 6, 7].

Studying solar flares, Dungey assumed in 1953 [8] that magnetic field lines can be broken and reconnected; in the early 1960s, he applied the reconnection concept to describe the interaction of solar wind with the Earth's atmosphere [9]. Although the physics of this phenomenon is not fully understood even now, the reconnection process is believed to be responsible for the transfer of mass, momentum, and energy from the solar wind to the magnetosphere, and also for the excitation of magnetic convection. The leading role of the magnetic reconnection mechanism finds support, in particular, in the well-established dependence of the magnetic field and plasma convection in the magnetosphere on the direction of the IMF in an unperturbed solar wind flow [10, 11]. In addition, there are direct observations of phenomena related to the reconnection in the Earth's magnetopause [12–18].

In the laboratory and magnetospheric plasmas, as well as on the Sun, a change in the magnetic field geometry and the appearance of streams of accelerated particles are observed over a time that is markedly shorter than that of ordinary magnetic field diffusion. These observations are explained by reconnections. The reconnection is also invoked to explain the viscous dissipation in accretion disks. A widely used approach to the reconnection problem is based on the MHD theory and consists in searching for a geometric configuration that would essentially shorten the effective dissipation time

[3]. However, as noted in [19], the physics of reconnection goes beyond the MHD approximation and calls for a kinetic approach.

The occurrence of neutral points is characteristic of magnetic fields having multiple sources. The locations where the magnetic field vanishes are called neutral or null points [3]. Neutral points in a plasma, as a rule, lead to the formation of current sheets. Specific dissipation regions evolve around neutral points. Two types of plasma moving toward each other through a dissipation region bring the magnetic field lines there. Their frozen-in state is violated in this region; they reconnect and are carried away by the plasma streams. The result is a redistribution of magnetic fluxes. The self-consistent dynamics of a highly conducting plasma are arranged such that neutral points of the magnetic field coincide with neutral points of the velocity field [20].

An essential contribution toward understanding the reconnection process was made by S I Syrovatsky (see, e.g., [21]). He was the first to theoretically consider a general nonstationary problem of the flow of a highly conducting compressible plasma in nonuniform magnetic fields containing neutral lines. He arrived at the conclusion that both the considerable increase in the electric current density in the vicinity of a neutral line and the accumulation of electric current in current sheets are possible. Plasma flows in strong magnetic fields, in particular, in the presence of neutral lines of a magnetic field, were investigated in [22, 23].

Since the 1960s, current sheets that appear in a compressible plasma flowing in an inhomogeneous magnetic field containing a neutral line were experimentally studied in the Accelerator Laboratory of the Lebedev Physical Institute (the problem was formulated by Syrovatsky). In a two-dimensional configuration, a line can exist such that the magnetic field has an X-type configuration in the plane perpendicular to it, while the field magnitude decreases to zero. This line is called the neutral or null line of the magnetic field. In the plane perpendicular to it, flows and the behavior of field lines are analogous to those of a two-dimensional reconnection [3]. As a result of these studies, a fundamental conclusion was drawn on the feasibility of magnetic energy accumulation if a current sheet is formed in the vicinity of a neutral line. The subsequent release of the accumulated magnetic energy occurred through an abrupt breakup of the sheet and was accompanied by the generation of pulse electric fields accelerating charged particles.

The concept of dynamic current sheets first introduced by Syrovatsky turned out to be very fruitful in solving numerous problems in the physics of laboratory and space plasmas. For example, it was shown that the Earth's magnetospheric tail evolves into a quasistable state in which the location of the far X-line oscillates between 40 and $60R_{\rm E}$ [19], where $R_{\rm E} = 6378.1$ km, the Earth radius.

The topology of magnetic fields plays a key role for astrophysical and laboratory plasmas, their dynamics, equilibrium conditions, and energy redistribution. Two configurations $\mathbf{B}_1$ and $\mathbf{B}_2$ are said to be topologically reducible if there is a motion transforming $\mathbf{B}_1$ into $\mathbf{B}_2$ and vice versa without violating their frozen-in character. Configurations $\mathbf{B}_1$ and $\mathbf{B}_2$ are considered topologically different if they are not topologically reducible. In this case, if the transition from $\mathbf{B}_1$ to $\mathbf{B}_2$ is feasible, it is accompanied by a change in topology and involves Ohmic dissipation [24].

Depending on the mutual orientation of the planetary magnetic field and IMF vectors, both two- and three-dimensional reconnections occur in planetary magnetospheres. A two-dimensional reconnection occurs at a neutral line, where the magnetic field decreases to zero, or at a quasineutral line, where only the component of the magnetic field along this line differs from zero. A three-dimensional reconnection occurs at a neutral point of the magnetic field [25–29]. A strictly two-dimensional reconnection is realized, for example, when the IMF and the axis of the dipole of the planet intrinsic magnetic field are parallel [30], and occurs at a neutral line lying in the magnetic equator plane. If the IMF component parallel to the planet dipole axis is strong and other components are small but nonzero, it can be shown that the two-dimensional reconnection also occurs at a quasineutral line [27, 28]. The field in the vicinity of the quasineutral line has the X-type topology in planes perpendicular to it.

If the prevailing component of the IMF is antiparallel to the planet dipole axis, then a three-dimensional reconnection occurs at neutral points of the magnetic field located near the cusps. This type of reconnection is characterized by a far more complex topology [16, 27, 31, 32]. Neither a quasineutral line nor an X-type configuration in the magnetic field are formed in the magnetosphere in this case.

The two-dimensional and three-dimensional reconnection types imply essentially different structures of the magnetospheric magnetic field and, consequently, magnetospheric convective flows and polar auroras. Accordingly, comparing theoretical concepts with observations is only possible if the reconnection type is known in each particular case. Such a comparison provides an adequate answer to the question about the influence of the interplanetary magnetic field on planetary magnetospheres.

It was argued in [14] that within the diffusion region, the freezing-in condition $\mathbf{E} + [\mathbf{V} \times \mathbf{B}] = 0$ is first violated on the scale of the order of the ion inertial wave $\lambda_{\rm i} = c/\omega_{\rm pi}$, where c is the speed of light and $\omega_{\rm pi}$ is the plasma ion frequency. There, ions are no longer magnetized, but electrons remain attached to the magnetic field. Further, on the scale of the electron inertia wave $\lambda_{\rm e}$, the electrons also lose magnetization. In the electron diffusion region, there exists an electric field aligned with magnetic field lines, $E_{\parallel} = \mathbf{E}\,\mathbf{B}$.

In the diffusion region, the current sheets separating magnetic field lines of different topological types (separatrix surfaces) intersect. The bounding separatrix surfaces host not only field-aligned currents but also field-aligned potential differences of the electric field and $E_{\parallel}$. Thus, small-scale structures considered in [17, 18] as diffusion zones are formed along the separatrix sheets. Recently, measurements inside or in the vicinity of diffusion zones, including the narrow layers along separatrix surfaces, were carried out for the Earth's orbit. For example, data of numerous measurements in regions of the size of the electron inertial length with a significant electric field $E_{\parallel}$ directed along the separatrices were presented in [17]. The observations indicate that the diffusion zones are of the order of $4-5\lambda_{\rm i}$ in size (in the vicinity of the Earth, $\lambda_{\rm i} \sim 100$ km).

The Cluster project [33] has been devised for performing simultaneous measurements at four spatial locations. Its main goal is to explore small-scale three-dimensional structures in the Earth magnetosphere and solar wind near the Earth. Satellites of the Cluster group have first discovered elongated electron diffusion regions stretching over 3000 km in the magnetosheath of the Earth magnetosphere [34]. In addition, they enabled the first observations of the structure of the magnetic field near the neutral point in the magnetotail [35].

The reconnection may proceed as a quasistationary or a sporadic process. Since the discovery of flux transfer events, various short and quasiperiodic events in the day auroral zone have been identified as the ionospheric manifestations of sporadic reconnection. Quasistationary reconnection in the Earth's magnetic field (with the dipole moment directed to the south) for the southward magnetic field of the solar wind was first predicted in [30]; the magnetosphere was regarded there as a time-averaged configuration.

According to [6], the idea of reconnection was very fruitful in explaining a number of phenomena in the laboratory and space plasmas and allowed identifying common features in processes spanning many orders of magnitude and differing in geometry and energy scales. The qualitative role of the reconnection idea is therefore immense, but its quantitative side has not reached maturity. Accordingly, the most valuable contribution presently comes not from theoretical models of reconnection but from ideas expressed through them, in particular, ideas pertaining to the formation of current sheets and the subsequent reconnection involving them.

Although the energy density of the interplanetary magnetic field is noticeably lower than the kinetic energy density of the solar wind and the magnitude of the IMF is lower than planetary magnetic fields by several orders of magnitude, the reconnection processes are indispensable in forming the global structure and dynamics of magnetospheres. The electric field and plasma of the solar wind can penetrate the magnetosphere along the reconnected magnetic field lines.

Table 1 presents characteristics of Solar System planets (the material in Ref. [36] was specifically used for the compilation). Mercury, Venus, the Earth, and Mars are the planets of the terrestrial group, showing similar size, mass, and bulk composition. Jupiter, Saturn, Uranus, and Neptune are giant planets, massive celestial bodies having no rigid surface and composed mainly of hydrogen and helium. About 98% of the net mass of Solar System planets is comprised by the giant planets, characterized by large sizes and masses, a relatively low density, fast rotation, strong magnetic fields, and numerous moons. Almost all the kinetic energy of the Solar System is attributed to the giant planets.

Table 1. Characteristics of the planets.

Planet	Radius R_p, km	Mean density, g cm^{-3}	Period of revolution around planet's axis, Earth days	Dipole moment, G R_p^3	Distance from the Sun, AU
Mercury	2439.7	5.43	58.6462	0.0033	0.39
Venus	6051.8	5.24	−243.0185	—	0.72
Earth	6378.1	5.515	0.9973	0.3	1.00
Mars	3397	3.94	1.0259	$< 1 \times 10^{-4}$	1.52
Jupiter	71,492	1.33	0.4135	4.28	5.20
Saturn	60,268	1.70	0.4440	0.21	9.58
Uranus	25,559	1.25	−0.7183	0.23	19.18
Neptune	24,764	1.64	0.6712	0.13	30.02

The rotation of most planets in the Solar System proceeds in the direction of their orbital motion. However, Venus rotates in the opposite sense. A single rotation of Venus around its axis takes 243 Earth days, which exceeds its siderial rotation period (Venusian year), lasting 224.7 terrestrial days. Uranus and Pluto also rotate in the opposite sense, but, in contrast to other planets, their rotation axes make only a small angle to their orbital planes, such that Uranus and Pluto behave as if they were 'rolling over.' In 2006, the International Astronomical Union designated Pluto a dwarf planet, not a classical planet of the Solar System.

The intrinsic magnetic field of a planet is a very important characteristic from the standpoint of space electrodynamics. Presently, the magnetic fields of all planets in the Solar System are known more or less reliably (see Table 1). Mercury's magnetic field is much smaller than the Earth's. Venus has no intrinsic magnetic field. The situation with Mars remains only partially clarified to date: even if it has a magnetic field, it is bound to be very small. For planets lacking intrinsic magnetic fields, the inductive interaction with the magnetized plasma of the solar wind becomes significant, entailing the formation of inductive magnetospheres.

For Jupiter, Saturn, Uranus, and Neptune, not only the mere existence of magnetic fields is well established, but also their multipole terms are known. The interaction of the solar wind with planetary magnetic fields results in the formation of large-scale magnetospheric magnetic and electric fields, convection, and current systems. For rapidly rotating giant planets having strong magnetic fields (Jupiter and Saturn), the rotation essentially shapes their magnetospheres and the character of their interaction with the solar wind.

2. Earth's magnetosphere

Earth is the largest among the planets of the terrestrial group. It contains an iron core, soft mantle, and solid crust. The mean density of the Earth's matter is 5.5 g cm^{-3}. The Earth's relief experiences variations within 20 km, including oceanic trenches. The mean distance from the Earth to the Sun, 1.5×10^8 km, has been adopted as 1 astronomical unit (AU). The Earth orbits the Sun at the mean speed 30 km s^{-1}. The angle between the polar axis and the plane perpendicular to the Earth's orbit (the ecliptic plane) is 23°. Owing to this inclination, the Earth has seasons. The annual mean temperature on the Earth is approximately 290 K. The Earth has the strongest magnetic field among planets of the terrestrial group, and its dipole moment is 0.3 G R_p^3 and is directed southward (R_p is the planet radius).

The Earth is surrounded by a magnetosphere, inside which the magnetic field plays a defining role, while the solar wind dominates outside. The mean plasma density in the Earth magnetosphere is $n_{\rm msph} = 2$ cm^{-3} and its mean temperature is $T_{\rm msph} = 20 \times 10^6$ K. The magnetospheric plasma is therefore more rarefied and hotter than the solar wind plasma. In addition to the Earth's intrinsic field, the magnetospheric current systems [37] serve as sources of the magnetic field in the magnetosphere.

A schematic of the Earth magnetosphere is presented in Fig. 1 (see also Refs [38, 39] and Fig. 7 in [40]). It shows the solar wind flow past the magnetosphere bounded by the magnetopause, which hosts the shielding currents. The thickness of the magnetopause is several ion gyroradii [39], or 400–800 km on the average [41]. The minimum magnetic field is found in high latitudes in the region of cusps. The IMF partly penetrates the magnetosphere. Below the magnetopause are the mantle, the tail lobes (the schematic displays only the northern lobe), and the plasma sheet enveloping the neutral current sheet of the magnetotail, with cross-tail

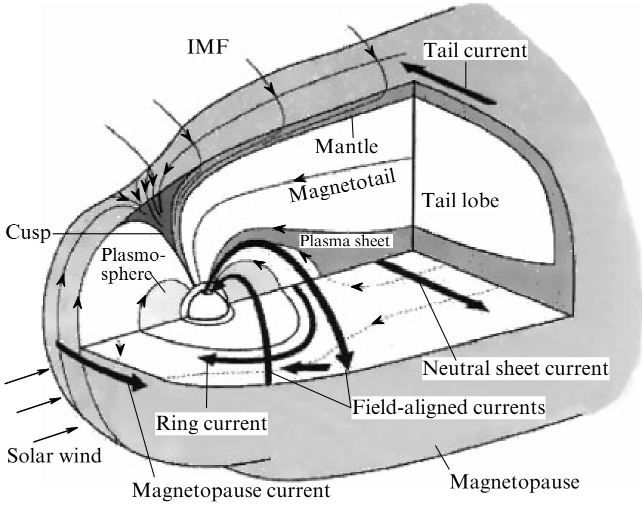

Figure 1. Schematic of the spatial structure of plasma, magnetic field, and electric currents in the Earth's magnetosphere.

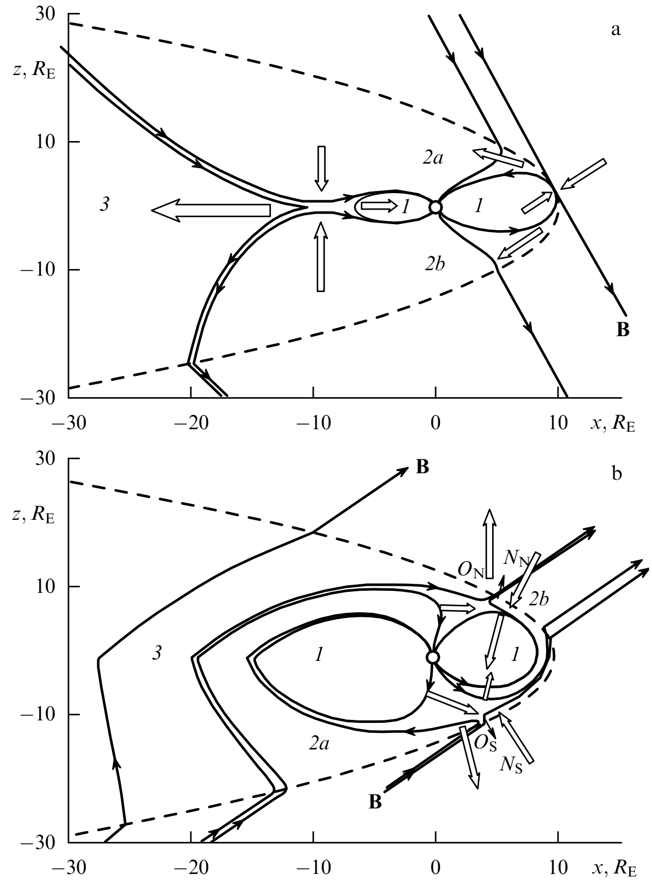

Figure 2. Magnetic field lines in the meridional noon–midnight section (computations are based on the paraboloid model of the magnetosphere). (a) The IMF vector points southward. A two-dimensional reconnection occurs along a low-latitude quasineutral line. The IMF components penetrating into the magnetosphere: $b_x = 0.8$ nT, $b_y = 0$ nT, $b_z = -2.8$ nT, $b \approx 3$ nT [27]. (b) The IMF vector points northward. A three-dimensional reconnection occurs at two neutral points of the magnetic field located near the cusps. The IMF components penetrating into the magnetosphere: $b_x = 0.8$ nT, $b_y = 0$ nT, $b_z = 2.8$ nT, $b \approx 3$ nT [27].

currents directed from dawn to dusk and closing on the magnetopause flow. The energy of ions in the plasma sheet of the magnetotail reaches $\sim 1-10$ keV. The Earth is surrounded by a plasmosphere, a region $4-6\,R_E$ in radius, where the plasma, primarily of ionospheric origin, rotates together with the Earth. This happens because the magnetic field lines are frozen in the ionospheric plasma. Collisions of the ionospheric plasma with neutrals at the altitude $\sim 120-140$ km redistribute the rotation to the magnetosphere. The density of a relatively cold plasma in the plasmosphere is about 10^2-10^3 cm^{-3}; outside the plasmosphere, the plasma is hotter and less dense, and, instead of rotation, the dominating motion becomes convection, generated by the interaction of the magnetosphere with the solar wind. The trap created by the Earth's magnetic field confines energetic particles, which build the Earth's radiation belts [42]. The centrifugal and magnetic drifts of energetic particles in the dipole field form a ring current. The electric currents along magnetic field lines set up sheets linked to polar auroras.

Because of the rotation of the Sun, the IMF is twisted into a large-scale spiral structure (Parker's Archimedes spiral). Close to the Earth orbit, the magnitude of the IMF is about ~ 5 nT under quiet conditions, whereas the magnitude of the geomagnetic field at the Earth equator is $\sim 3 \times 10^4$ nT. Nevertheless, the magnetic field of the solar wind plays a decisive role in the physics of the Earth magnetosphere. The magnetic field of the solar wind radically changes the structure of the Earth's magnetospheric magnetic field, the changes being affected by the direction of the IMF [27, 28, 43–49]. The high magnetic pressure of the solar wind and the IMF directed southward strongly augment the energy and momentum transfer to the magnetosphere. The magnetic variability of the magnetosphere is characterized by the geomagnetic activity indices (*Kp*, *AE*, and others).

The reconnection requires that at least three conditions be satisfied: neutral lines or neutral points of the magnetic field exist, a highly conducting plasma is present, and some perturbation of the initial equilibrium state occurs that initiates magnetohydrodynamic flows in the plasma and leads to the excitation of electric current. As mentioned in [6], the convergence of magnetic field lines with essentially different directions of the magnetic field implies that the current density has to be sufficiently high near the convergence point and that a finite conductivity is actuated upon reconnection only in compact regions with high current density, with the change in the topology of field lines occurring there affecting the motion of all the plasma.

When the IMF is directed southward, a two-dimensional reconnection occurs at a low-latitude quasineutral line. For the northward direction, the reconnection bears essentially a three-dimensional character and occurs at neutral points near the cusps [10, 16, 27, 28, 46, 50, 51]. As a result of reconnection, large-scale convection is excited in the magnetosphere, which corresponds to cyclic motion of the plasma (the formation of open field lines from interplanetary and closed ones, and then the formation of interplanetary and closed ones from open field lines of the two polar caps). On the level of the ionosphere, a two-vortex convection pattern emerges for the southward IMF and a four-vortex one for the northward IMF (see, e.g., [28]).

Figure 2 [27] shows the magnetic field lines of the Earth magnetosphere in the meridional noon–midnight cross section (the Sun is to the right) for the vector of the IMF directed southward (Fig. 2a) and northward (Fig. 2b). The plasma flows are indicated by large arrows. Figures 2a and 2b respectively correspond to the two- and three-dimensional reconnection. O_N and O_S are the neutral points located in the north and south cusps, and N_N and N_S are the outer normals to the magnetopause at the neutral points. The magnetopause is plotted by the dashed line. The digits mark field lines of different types: *1* stands for closed field lines emanating from and ending at the Earth, *2a* and *2b* are the open field lines respectively connecting the interplanetary space with the north and south polar caps, and *3* are interplanetary field lines penetrating into the magnetosphere.

The first reconnection process occurs at the location where the interplanetary and closed magnetospheric lines first meet. The outcome is the open field lines of two polar caps carried tailward by the solar wind. The inverse reconnection process occurs where the open field lines of two polar caps reconnect on encountering each other, which brings back the interplanetary and closed field lines. The cycle is thus closed.

Figure 3 [27] presents the reconnection in the case where the IMF direction is close to the radial one, i.e., the radial component directed toward (Fig. 3a) or from (Fig. 3b) the Sun is greater than or equal to the north–south component of the IMF. The azimuthal component of the IMF is zero in Figs 2 and 3. If the direction of the IMF is close to the radial one, the reconnection in the magnetosphere occurs simultaneously at the neutral point in the cusp vicinity and on the line — a fragment of separatrix C_2 (shown by the solid curve in Fig. 3) located at the magnetopause near the second cusp. The separatrix is composed of two magnetic field lines: C_1 (not shown in the figure) and C_2 connecting the neutral points. Figures 2 and 3 are based on computations carried out with the paraboloid model of the Earth magnetosphere [52]. For better visualization, the IMF was taken to be of the order of 30 nT [27].

In the paraboloid model of the magnetosphere, the magnetopause is approximated by a paraboloid of revolution. The main sources of the magnetic field in this model are the Earth magnetic field, the tail current system, the ring current, and the shielding current of the magnetopause. The paraboloid model also accounts for a partial penetration of the IMF into the magnetosphere. The portion of the interplanetary magnetic field penetrating into the magnetosphere amounts to 10–20%. The computations are routinely carried out in the geocentric solar magnetospheric (GSM) system of coordinates with the X axis directed sunward and the Y axis perpendicular to the Earth magnetic dipole and directed toward the dusk, such that the dipole axis is in the XZ plane. The angle Ψ between the dipole axis and the plane perpendicular to the Earth–Sun line is called the dipole tilt angle. Positive values of Ψ are associated with winter in the Northern Hemisphere, and negative, with summer. The angle Ψ depends on the time, day number, and season as

$$\sin\Psi = -\cos\alpha_1 \sin\beta_2 + \sin\alpha_1 \cos\beta_2 \cos\varphi_m\,, \tag{2}$$

where $\alpha_1 = 11.43°$ is the tilt angle between the magnetic dipole and the Earth's rotation axis, β_2 is the inclination of the Sun, which depends on the day of a year, and φ_m is the angle between the plane of the midnight meridian and the meridional plane containing the north pole of the Earth dipole. The magnitude of φ_m depends on the universal time UT: $\varphi_m = \pi((\mathrm{UT}/12^h) - (l_n/180°))$, where l_n is the geographical longitude of the northern geomagnetic pole. During a

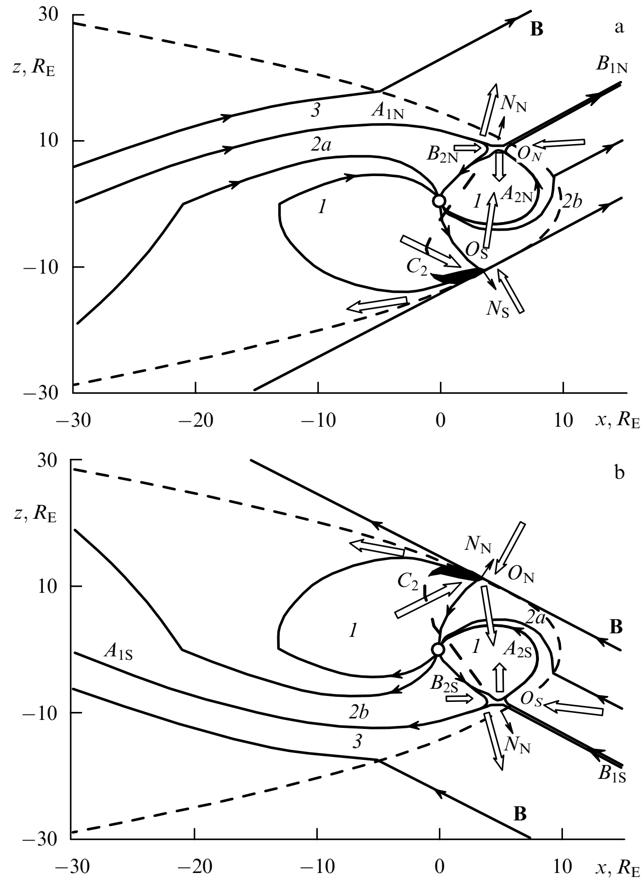

Figure 3. (a) Magnetic field lines in the meridional noon–midnight section for the IMF vector with a strong radial component directed toward the Sun, computed in the framework of the paraboloid model of the magnetosphere. Both the two-dimensional reconnection along a fragment of separatrix C_2 lying at the magnetopause and passing through the southern neutral point, and the three-dimensional reconnection at the northern neutral point occur. The IMF components penetrating into the magnetosphere: $b_x = 2.2$ nT, $b_y = 0$ nT, $b_z = -2.0$ nT, $b \approx 3$ nT. (b) The same as in (a), but for the IMF vector with a strong radial component directed from the Sun. Here, the two-dimensional reconnection along a fragment of separatrix C_2 lying at the magnetopause and passing through the northern neutral point and the three-dimensional reconnection in the southern neutral point occur. The IMF components penetrating into the magnetosphere: $b_x = -2.2$ nT, $b_y = 0$ nT, $b_z = 2.0$ nT, $b \approx 3$ nT [27].

year, Ψ varies within $\pm 35°$, and during a day, within $\pm 11.43°$ with respect to the mean value equal to $-\beta_2$.

The size of the magnetosphere is characterized by the distance R_1 from the center of the planet to the point of the magnetopause that is closest to the Sun (subsolar point). For the Earth, $R_1 = 10R_E$ on average, the distance to the bow shock wave is about $14R_E$, and the geomagnetic tail stretches as far as $1000R_E$ (according to Pioneer 7 data). In the far part of the magnetotail, the magnetic pressure in the tail lobes is balanced by the thermal pressure of the magnetosheath plasma. According to observations, the mean radius of the far magnetotail is about $30R_E$, whereas the magnetic field magnitude in tail lobes is ~ 9.2 nT [53]. The mean geocentric distance to the internal edge of the current sheet is $R_2 \approx 7-8R_E$. The electric field potential difference across the magnetotail is about 20–50 kV (for a strong southward IMF, up to 100 kV).

The paraboloid model of the magnetosphere [52, 54] is a dynamical model describing both the internal and external magnetospheres with good accuracy, even during the periods of perturbed activity. It proposes both a physical and analytic description of the Earth's magnetospheric magnetic field. The magnetic field is defined as a vector sum of fields of the main current systems specified in terms of the input parameters of the model. The input parameters are derived from observations taking the conditions inside the magnetosphere and within the solar wind into account. All the internal magnetospheric sources are shielded by currents at the magnetopause. The total magnetic field vector $\mathbf{B}(x, y, z)$ at a spatial location (x, y, z) inside the magnetosphere is expressed in the heliomagnetospheric coordinate system at time t as

$$\mathbf{B}(t) = \mathbf{B}_{\mathrm{d}}(\Psi) + \mathbf{B}_{\mathrm{cf}}(\Psi, R_1) + \mathbf{B}_{\mathrm{T}}(\Psi, R_1, R_2, \Phi) + \mathbf{B}_{\mathrm{r}}(\Psi, b_{\mathrm{r}}) + \mathbf{B}_{\mathrm{sr}}(\Psi, b_{\mathrm{r}}, R_1) + \mathbf{B}_{\mathrm{FAC}}(\Psi, R_1, J_0)\,, \quad (3)$$

where $\mathbf{B}_{\mathrm{d}}(\Psi)$ is the Earth's intrinsic magnetic field, $\mathbf{B}_{\mathrm{cf}}(\Psi, R_1)$ is the field due to currents at the magnetopause that shield it, $\mathbf{B}_{\mathrm{T}}(, R_1, R_2, \Phi)$ is the field of the tail current system composed of currents across the tail and their closures on the magnetopause, Φ is the magnetic flux in the tail lobes, $\mathbf{B}_{\mathrm{r}}(\Psi, b_{\mathrm{r}})$ is the field of the ring current, b_{r} is the magnitude of the magnetic field due to the ring current at the Earth's equator, $\mathbf{B}_{\mathrm{sr}}(\Psi, b_{\mathrm{r}}, R_1)$ is the field of currents at the magnetopause that screen the ring current, and $\mathbf{B}_{\mathrm{FAC}}$ is the field of field-aligned currents (it is not taken into account in figures in this review). The field $\mathbf{B}_{\mathrm{cf}}$ is determined by solving the von Neumann problem for the potential U_{cf}, i.e., $\mathbf{B}_{\mathrm{cf}} = -\nabla U_{\mathrm{cf}}$ with the boundary condition $\mathbf{B}_{\mathrm{cf}} \times \mathbf{n} = -\mathbf{B}_{\mathrm{d}} \times \mathbf{n}$, where $\mathbf{n}$ is the normal to the magnetopause. The magnetic field of the tail current system $\mathbf{B}_{\mathrm{T}}$ is determined in terms of the scalar potential $\mathbf{B}_{\mathrm{T}} = -b_{\mathrm{t}} R_1 \nabla U_{\mathrm{t}}$, where $b_{\mathrm{t}} = (2F/(\pi R_1^2))(R_1/(R_1 + 2R_2))$ is the magnitude of the magnetic field of tail currents at the forward edge of the current sheet R_2. The expansion of potentials U_{cf} and U_{t} in series in spherical harmonics or Bessel functions is described in detail in Ref. [55]. To compute $\mathbf{B}_{\mathrm{r}}$, the vector potential $\mathbf{A}$ ($\mathbf{B}_{\mathrm{r}} = \nabla \times \mathbf{A}$) is introduced. The modeling of field-aligned currents is described in Ref. [56]. It is assumed that the outer boundary of the ring current outside which its density vanishes coincides with the internal boundary of the tail current sheet R_2, and that the ring current has only an azimuthal component. Computation of the field due to the currents screening the circular current was carried out under the assumption that the normal component of the magnetic field is zero at the magnetopause. The input parameters of the model include the geomagnetic indices *Dst* and *AL*, Φ, R_1, R_2, Φ, b_{r}, and J_0 (the total density of field-aligned currents). A thorough description of the paraboloid model and its comparison with other models of the Earth magnetosphere is given, e.g., in Ref. [57].

We list some of the well-known models of the Earth's magnetosphere magnetic field. They include the model of Mead and Fairfield [58], the model of Olson and Pfitzer [59], the T87 [60] and T89 [61] models of Tsyganenko, the model of Hilmer and Voigt [62], the T96 [63] model of Tsyganenko, the paraboloid model [54], the model of Maltsev and Ostapenko [64], and the T01 [65] model of Tsyganenko. In the Mead–Fairfield and Maltsev–Ostapenko models, a separate description of large-scale magnetospheric current systems is lacking. Only their net magnetic field is computed, which does not allow following the evolution of each current system having a specific reaction time to changes in the solar wind, as is allowed by the paraboloid model. The Mead–Fairfield and T87 and T89 models use the *Kp* index characterizing the intensity of magnetic perturbations every 3 hours, which prohibits a detailed description of faster variations in the magnetic field and magnetospheric dynamics, in particular, during magnetic storms (the paraboloid model permits simulations of magnetospheric dynamics on a time scale exceeding 15 min, including the perturbed periods). In the Olson–Pfitzer model, the shape of the magnetopause was found empirically, whereas the distance to the subsolar point of the magnetopause was scaled depending on the magnetospheric activity; the ring current, currents at the magnetopause, and the tail current were scaled according to this distance (the magnetosphere scale R_1 in the paraboloid model depends on the parameters of the solar wind and the IMF).

The T89 model incorporates 6 statistical models for various levels of the *Kp* index. It is designed to model perturbed periods and is based on an empirical description. It lacks the boundary between the ring and tail currents; the magnetopause is not associated with a surface (the screening currents of the paraboloid model are absent). The Hilmer–Voigt model uses four physical parameters to specify three current systems: the ring, the tail, and magnetopause currents. The magnetopause is modeled as a surface composed of a semi-infinite cylinder and the day hemisphere of equal radii. The magnetopause currents shield only the dipole. The internal edge of the magnetotail plasma sheet is located at $10.5R_{\mathrm{E}}$. T96 is an improved version of T87 and T89. The input parameters of the T96 empiric statistical model are the dipole tilt angle, the *Dst* index, the dynamic solar wind pressure, and the IMF components B_y and B_z. The model relies on magnetic field measurements by satellites at distances from $3R_{\mathrm{E}}$ to $70R_{\mathrm{E}}$ (the paraboloid model allows computations in more distant parts of the tail). The magnetopause is specified as a semi-ellipsoid transforming into a cylinder. The magnetopause screens the dipole, the ring current, and tail currents. T01 is a modification of the series and is used most frequently. It relies on empirical measurements of the magnetic field by satellites near the Earth (at $x > -15R_{\mathrm{E}}$). The magnetic field is computed as a vector sum of fields due to the main magnetospheric current systems specified in terms of a large set of parameters, which do not always suggest a simple physical interpretation. The paraboloid model accounts for the penetration of all IMF components into the magnetosphere. Full screening of all magnetospheric sources by magnetopause currents has a defining impact on the rigorous account of the influence of a relatively weak IMF on the structure of the magnetosphere.

Very large structures of solar matter in the form of plasma blobs carrying a frozen magnetic field and ejected from the Sun to the heliosphere at speeds from several hundred to more than 1000 km s^{-1} are called coronal mass ejections (CMEs). The CME is the strongest manifestation of solar activity [66]. Sufficiently strong CMEs move much faster than the solar wind and generate a shock wave ahead of them. An encounter of the magnetosphere with shock waves or fast streams in the solar wind can trigger a magnetic storm in the magnetosphere [67]. The magnetic storm is characterized by a global perturbation of the geomagnetic field, which is manifested as a reduction in the magnitude of the northward field component in the Earth's equatorial belt (by 100 nT or even more on average). The characteristic time of the magnetic storm cycle is about $1/2$ day, whereas recovery of equilibrium takes several subsequent days. During a magnetic storm, a significant amount of ions and electrons is injected into the Earth's radiation belts; the global reduction in the magnetic field magnitude implies amplification of the tail and ring currents [68]. In this case, the energy of the ions in the ring current lies in the range $\sim 10-300$ keV. To characterize the magnetic storms, the *Dst* index was introduced. It describes the mean perturbation of the magnetic field measured by several observatories near the equator. During strong geomagnetic storms, the potential difference across the polar cap increases from 40 kV in quiet conditions to 150–200 kV [69]. Magnetic storms occur relatively seldom. Much more frequent are magnetospheric substorms.

In the course of a magnetospheric substorm (with the characteristic time scale about one hour), the energy of the solar wind accumulated earlier in the geomagnetic tail is released in an explosive way and is channeled into the internal magnetosphere and polar ionosphere, partly leaking into the plasma kinetic energy or heat. This is accompanied by strong geomagnetic perturbations. Several intense substorms sometimes occur as a magnetic storm unfolds. A substorm begins when a large amount of energy is accumulated in the tail lobes, which commonly happens when the southward IMF ($\geqslant 10$ nT) persists for three or more hours. The total energy turnover of a substorm reaches 10^{15} J, and that of the magnetic storm, $10^{16}-10^{18}$ J [1].

A terrestrial manifestation of a substorm is an abrupt intensification of polar auroras in the midnight sector. As the substorm begins, the auroral arches gain in brightness, move rapidly to the pole, and intensively propagate. Their activity lasts for a half an hour and then decays. The polar auroras on the Earth are the light emission by the upper rarefied atmospheric layers caused by the interaction of atoms and molecules with streams of charged high-energy particles (electrons and protons) entering the Earth atmosphere from the magnetosphere or the interplanetary space. Light is emitted at approximately 100 km and higher above the Earth surface. Collisions of accelerated particles with neutral atoms in the upper atmosphere (oxygen and nitrogen) lead to the excitation of atoms, i.e., to their transition to a higher-energy state. They return to the equilibrium by emitting light quanta at certain wavelengths, which brings about polar auroras. Polar auroras often occur along geomagnetic field lines.

Streams of high-energy electrons linked to strong field-aligned currents flowing out of the ionosphere excite bright forms of discrete polar auroras seen with the naked eye. Less intense diffuse polar lights arise as a result of precipitation in the atmosphere of charged particles confined by the geomagnetic field and experiencing ordinary scattering without additional acceleration. The acceleration of electrons leading to discrete polar auroras occurs in a localized interval of heights located radially $2-3R_{\mathrm{E}}$ from the Earth surface. This is the electrostatic acceleration region, which, in addition to the field-aligned currents, contains an electric field directed along the magnetic field lines and accelerating the plasma. During substorms, an additional contribution comes from the Alfvén acceleration: the electromagnetic energy flux, directed toward the Earth and observed at the radial distances $4-6R_{\mathrm{E}}$ from the Earth surface, is sufficient to excite intense polar lights in lower regions. The Polar spacecraft observed the structure and dynamics of fluctuations of intense electric and magnetic fields related to Alfvén waves in this region at the boundary of the plasma sheet. In this case, the Poynting vector is directed along the magnetic field lines toward the ionosphere such that energy required to accelerate the plasma in the auroral zone is supplied there, leading to the observed generation of polar auroras. The details of the electron acceleration mechanism causing auroras are not clear presently [70]. The electric field aligned with the magnetic field supports a field-aligned current in the acceleration region, which is larger than could be assured by the available current carriers in the absence of additional acceleration.

The spectrum of polar auroras is composed of emission lines and bands. Some of the night sky emission lines, first and foremost the green and red lines $\lambda = 5577$ Å and $\lambda = 6300$ Å of atomic oxygen, are amplified there. Polar auroras observed in the optical band also contain molecular bands of N_2. Since the 1950s, the spectrum of polar auroras was also explored in the infrared and ultraviolet ranges. The emission energy in the infrared part of the spectrum is many times greater than that in the visible part. The term radioaurora is used to designate the auroral activity creating inhomogeneities of ionization oriented along the magnetic field lines at auroral heights and causing backscattering of radio waves.

A glowing oval of polar auroras with the mean radius $\sim 20°$ [71] occurs in the projection on the ionosphere. Polar auroras are most intense when the magnetic field is perturbed. The oval becomes broader when the geomagnetic activity is high. The geomagnetic field lines connect the boundary of the day sector of the polar aurora oval with the magnetopause. Polar auroras are dramatically amplified during magnetic storms: they can expand far beyond the oval characteristic of quiet states.

The NASA project THEMIS is aimed at exploring the origin of polar auroras. In the framework of the THEMIS mission, five satellites equipped with instruments to measure electric and magnetic fields and with detectors of electrons and ions were launched into a near-Earth orbit. These satellites allow monitoring the processes occurring in the magnetotail at various distances from the Earth at moments preceding the abrupt amplification of polar auroras and determining at which distance a perturbation occurs. A conclusion was drawn from observations that the most probable mechanism triggering substorms and, consequently, the acceleration of charged particles along the magnetic field lines and intensification of polar auroras is the reconnection in the geomagnetic tail at the geocentric distance $-20R_{\mathrm{E}}$ [72].

Figure 4 illustrates the excitation of polar auroras on the Earth as a result of the magnetosphere–ionosphere interaction [73]. Three major regions required for auroras to occur are shown: the magnetospheric dynamo, the ionospheric load, and field-aligned currents with an accelerating interval connecting them. The electric field is shown in Fig. 4 by equipotential surfaces having the shape of nested V's. At locations where the field-aligned component prevails, magnetic field lines may experience 'sliding.' The ionosphere is not a passive load: when charged particles (in particular, electrons that have passed through the accelerating region) impinge on the upper atmosphere, its ionization state and hence the conductivity changes.

The polar auroras depend not only on the level of magnetic activity in the Earth magnetosphere but also on the parameters of the solar wind and its magnetic field. Changes in the velocity and density of the solar wind, as well as in the magnitude and orientation of the IMF, involve

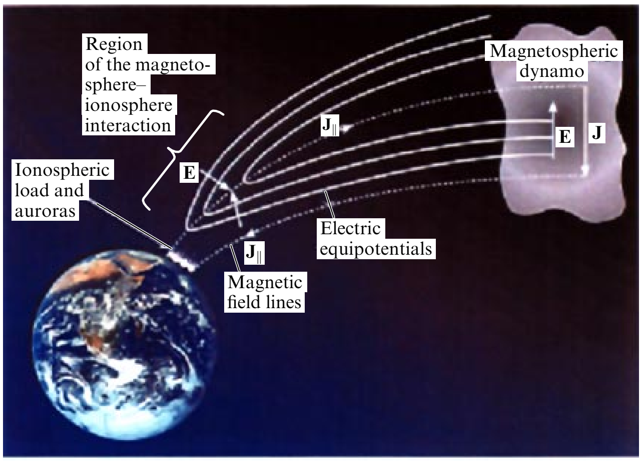

Figure 4. Schematic of the magnetosphere–ionosphere interaction generating polar auroras on Earth (see Ref. [73]).

changes in the sizes and shape of the magnetosphere, parameters of the main magnetospheric current systems and, as a consequence, the polar cap area and the magnitude of its magnetic flux. The strongest influence on the position of the polar aurora oval is exerted by the north–south component of the IMF. An increase in the south component results in a widening of the oval and its shift to lower latitudes [71]. Figures 5 and 6 demonstrate the dynamics of the polar cap (the region inside the oval of the polar auroras) as a function of the parameters of the solar wind and its magnetic field, using the events of 24–25 September 1998 as an example.

At approximately 23:45 UT on 24 September 1998, a coronal mass ejection carrying its magnetic field reached the Earth magnetosphere. In Fig. 5a, based on the data collected by the WIND/SWE spacecraft, we show (from top down) the thermal velocity V_{th}, the density of solar wind ions N, the components of the solar wind velocity V in GSM coordinates, and the dynamic solar wind pressure $p = nV_x^2$. The data from WIND/SWE were offset by 25 min, the time necessary for the CME to pass from the satellite located $184R_{\mathrm{E}}$ from the side of the Earth facing the Sun to the magnetopause. Because of a simultaneous increase in the velocity and density, the dynamic pressure of the solar wind jumped from 2 nPa to $\sim$ 15 nPa. The IMF also changed (Fig. 5b). The bottom plot presents the magnetic flux of the polar cap computed as the product of the polar cap area, provided by the Polar satellite (UVI, VIS), with the magnitude of the Earth magnetic field at the altitude of 120 km (56,000 nT) [74].

A sharp increase in the solar wind pressure leads to a reduction in the geocentric distance to the subsolar point of the magnetopause R_1, because the size of the day magnetosphere is inversely proportional to the solar wind dynamic pressure to the power one sixth [75]. Because R_1 is the characteristic spatial scale of the magnetosphere, its reduction is expected to be followed by a reduction in the geocentric distance to the inner edge of the current sheet (R_2), accompanied by an increase in cross-tail currents. This

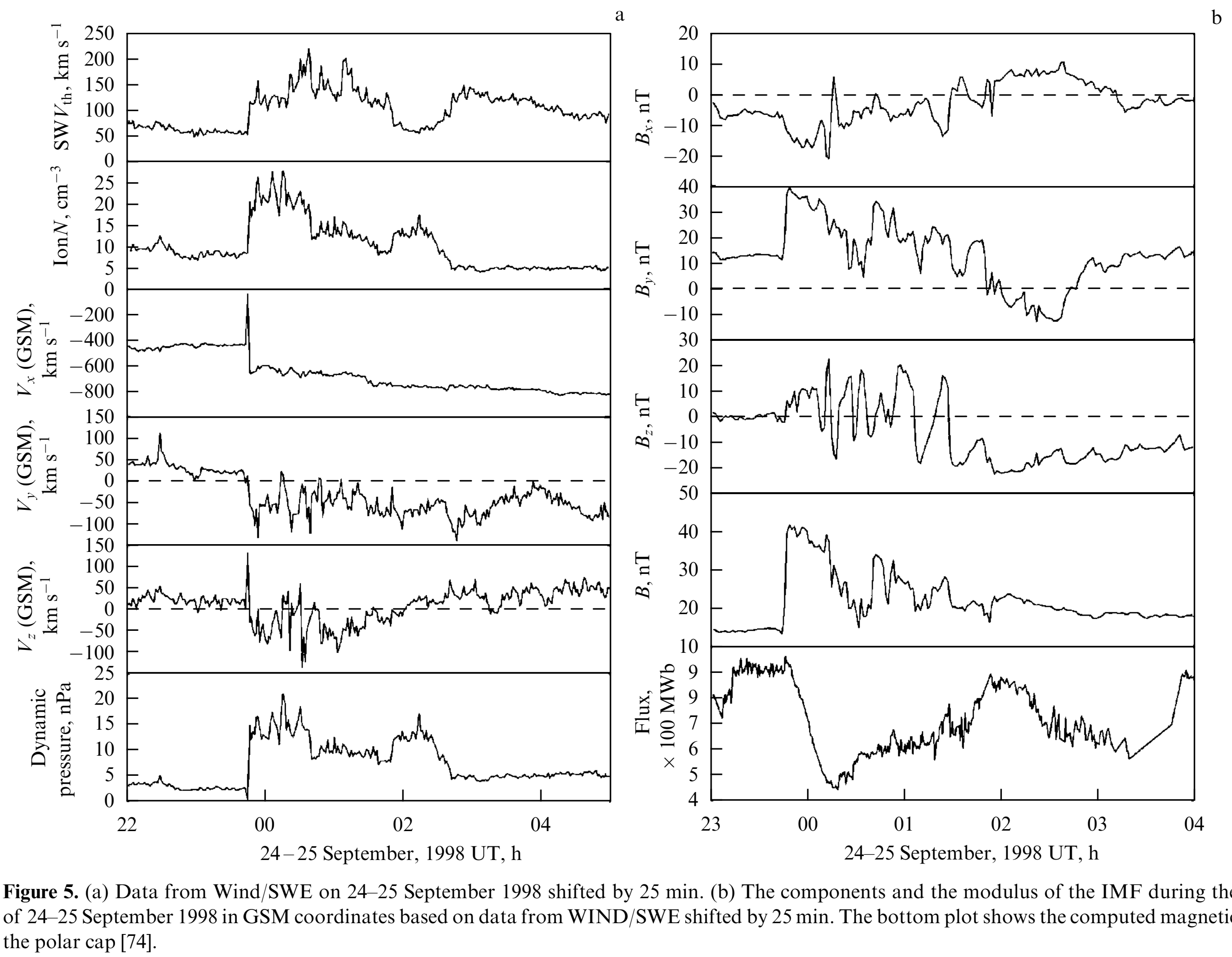

Figure 5. (a) Data from Wind/SWE on 24–25 September 1998 shifted by 25 min. (b) The components and the modulus of the IMF during the events of 24–25 September 1998 in GSM coordinates based on data from WIND/SWE shifted by 25 min. The bottom plot shows the computed magnetic flux of the polar cap [74].

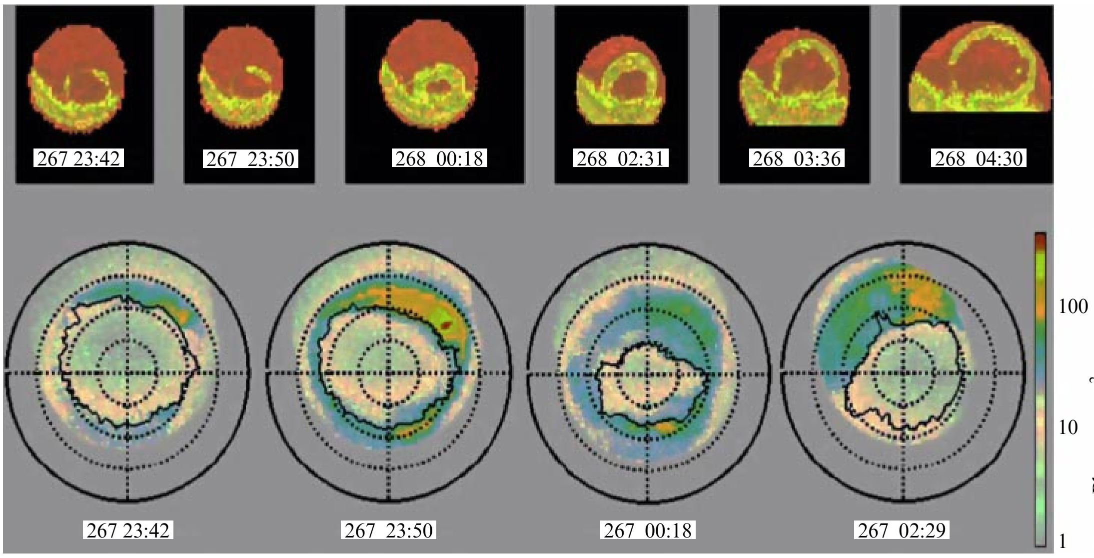

Figure 6. Data from the spacecraft Polar on 24–25 September 1998; the top row: images obtained with the VIS/Earth Camera; the bottom row: UVI images (the Sun is below) [74].

should lead to an increase in the polar cap area and the magnetic flux. However, this does not happen (see Fig. 6).

The B_z component of the IMF (see Fig. 5) turned to the south approximately 1 h 42 min after the arrival of the interplanetary shock wave to the magnetopause (it had had a mean north direction before). As can be seen from Fig. 2, the geometry of the tube of open magnetic field lines is strongly affected by the B_z component and for the northward IMF, the region of open field lines in the ionosphere (frequently identified with the polar cap) decreases in comparison with the southward IMF. This fact finds support in numerous observations. One of them is presented in Fig. 6. Its top part shows images taken with a visible imaging system (VIS), and the bottom one, with an ultraviolet imager (UVI). Figure 6 indicates that the polar cap decreased, the activity of the polar oval increased, and it expanded after the arrival of the CME. Hence, in the case considered, the size of the polar cap was stronger affected by the northward IMF than by the jump in the solar wind pressure. As the IMF turned southward, the polar cap began to grow. During the second hour of 25 September 1998, the main phase of the magnetospheric storm, which could be classified as one of the strongest, was unfolding: the variations in the *Dst* index were reaching 210 nT. The last three VIS images in Fig. 6 show the subsequent increase in the polar cap, the reduction in the oval width, and the spreading toward the equator of both oval sides, in agreement with the conservation of the southward component of the IMF and the development of a magnetic storm. During the turn of the IMF to the north on the arrival of the CME, the polar cap decreased twofold compared to the initial size; during the main storm phase, the polar cap increased threefold compared to the initial size. As the main storm phase was expiring, the auroras were losing their activity. As argued above, the change in the direction of the IMF primarily influences the reconnection locations, the topology of the magnetic field, the structure of magnetospheric current systems, and the size of the polar cap and the structure of convection there.

In addition to persistent large-scale magnetospheric current systems governed by the solar wind parameters, current systems of a short time scale, from 30 min to an hour, emerge under some conditions. Examples include the current wedge of a substorm [76] or a transition current system [74]. By the end of the growth phase and at the beginning of the expansion substorm phase, a so-called current wedge of the substorm develops. It consist of field-aligned currents closed by ionospheric currents and cross-tail currents in the plasma sheet of the near and middle magnetotails. In this case, the amplified current across the magnetotail closes to the ionosphere through field-aligned currents. Transition current systems arise in the high-latitude magnetosphere as a jump in the solar wind pressure impinges on the Earth's magnetosphere, accompanied by a simultaneous turn by the IMF from a nearly horizontal direction to the north [74].

3. Mercury's magnetosphere

Mercury is the nearest planet to the Sun and the smallest of the terrestrial group planets. Its radius is 2439.7 km. The mean distance to the Sun is 0.39 AU, the perihelion is 0.307 AU, and the aphelion is 0.467 AU. The advance of Mercury's perihelion, known with an accuracy of $\sim 1\%$, served as a test ground for the general relativity theory [77, 78]. Mercury's mean orbital speed is 48 km s^{-1}, and the planet orbits around the Sun in 88 Earth days. Mercury has the orbit with the strongest ellipticity; its eccentricity is 0.2. The rotation around its axis (stellar day) takes 58.6 Earth days and constitutes 2/3 of a Mercurian year. Mercury's rotation axis is nearly perpendicular to its orbit plane. The planet has no moons. Its relief is characterized by a height difference within 5 km. The maximum temperature on Mercury reaches 700 K. It is assumed that the planet has an iron core occupying $\sim 0.75 R_{\mathrm{M}}$ [78], which is surrounded by a mantle, followed by a silicate crust [36].

Observations of Mercury with the help of spacecraft have amounted to three flybys by Mariner 10 on 29 March and 21 September 1974 and 16 March 1975 and two flybys by the MESSENGER spacecraft (a NASA project) on 14 January and 6 October 2008. The next flyby of MESSENGER is planned for 29 September 2009. Then, it will complete almost four revolutions around the Sun to finally occur on the orbit of Mercury on 18 March 2011.

Mercury's magnetic field is weaker than the Earth's by two orders of magnitude; correspondingly, its magnetosphere is much smaller than the Earth's. The magnetic moment of the Mercury dipole is directed to the south, as on the Earth. The magnetic moment magnitude was estimated from the data of the first flyby of Mariner 10 as 351.5 ± 20.7 nT R_{p}^3, and the ecliptic latitude and longitude respectively as $-80 \pm 5°$ and $+285 \pm 10°$ [80]. Recent measurements conducted by MESSENGER supplied the new value 230–290 nT R_{p}^3 for the central dipole of Mercury, with the inclination of the rotation axis from 5 to 12° [81].

The Mercury magnetosphere is small and dynamic. Its size is only 5% of that of the Earth's magnetosphere. A characteristic convection time is 1 min, to be compared to about one hour for the Earth [82, 83]. Because of the weak magnetic field, the ion giroradius exceeds the distance R_1 from the planet center to the subsolar point of the magnetopause for mean-energy ions [84, 85]. The density ratio of the magnetospheric plasmas of Mercury and the Earth is approximately equal to the ratio of the solar wind plasma density on the orbits of Mercury and the Earth [83]. The results from the first flyby of MESSENGER showed that the Mercury magnetosphere is embedded in a comet-like cloud of planetary ions [86] of a complex composition with prevailing Na^+ ions [87].

Owing to the proximity to the Sun, the solar wind pressure and the magnitude of its magnetic field are by an order of magnitude larger for Mercury than for the Earth, and by two orders than for Jupiter [81, 88]. The mean pressure is ~ 20 nPa, and the IMF is of the order of 30 nT. Unlike for the Earth, the radial component dominates because the angle between the Archimedean spiral describing the IMF direction and the radial direction near Mercury is $\sim 20°$. Accordingly, the influence of the solar wind and the IMF on the Mercury magnetosphere is of paramount importance. Additionally, it is assumed that the coefficient of IMF penetration into the Mercury magnetosphere is 3–4 times larger than for the Earth [89]. The characteristic solar wind parameters are $V = 400$ km s^{-1} and IMF ~ 27 nT at the orbit point nearest to the Sun, i.e., the potential difference of the electric field applied to the day X-line $\sim 1.5R_{\mathrm{M}}$ in length is ~ 40 kV for the southward IMF. Under perturbed conditions ($V = 500$ km s^{-1}, IMF ~ 90 nT), the potential difference applied to the magnetosphere may reach 165 kV [90]. The IMF was directed northward during the first flyby of MESSENGER, and southward during the second one. The magnitude of the IMF was of the same order in both cases.

The analysis of the measurements performed by Mariner 10 and MESSENGER showed that Mercury's magnetosphere is similar in structure to the Earth magnetosphere. The mean distance from the planet center to the subsolar point of the magnetopause is $R_1 = 1.5R_{\mathrm{M}}$ for Mercury. Under the influence of variations in solar wind parameters, this distance changes, on average, from $1.3R_{\mathrm{M}}$ for the southward IMF to $2.1R_{\mathrm{M}}$ for the northward one [91]. Occasionally, the dayside magnetopause may approach the planet surface, but induction currents generated inside Mercury limit this motion [92]. The observed diameter of the Mercury magnetotail is $\sim 5R_{\mathrm{M}}$, to be compared with $40R_{\mathrm{E}}$ for the Earth [93].

Mercury is nearly void of atmosphere and ionosphere; the planet is enveloped by a tenuous exosphere, a thin gas shell consisting of neutral and ionized atoms of Na and K. It is supposed that there are two sources for the magnetospheric plasma, the solar wind and ionization of the neutral exosphere. During its first flyby, MESSENGER discovered that the magnetosphere is rich in various planetary ions of various ionization degrees [87]. It was noted in [94] that the Sun-illuminated hemisphere of Mercury is covered by a layer of photoelectrons, which may play the role of a horizontal conducting surface serving to close the field-aligned currents coupling the planet to its magnetosphere. The total conductivity of this layer is much smaller than those of the ionospheres of the Earth, Jupiter, and Saturn.

The polar caps on Mercury are the regions of open field lines connecting the planet to the solar wind. The radius of the near-equatorial boundary of the polar caps is $17-26°$ [95]. The IMF was directed predominantly northward during both the third flyby by Mariner 10 and the first flyby by MESSENGER. In both cases, a relatively quiet magnetospheric magnetic field was observed (as on the Earth under analogous conditions), accompanied by the absence of energetic particles [86]. In contrast, a strongly perturbed magnetospheric field and hot plasma were discovered along the part of the outbound Mariner 10 trajectory adjacent to the point where it left the magnetosphere during the first flyby. In this case, a southward IMF was detected in the magnetosheath. The situation was reminiscent of a substorm in the Earth magnetosphere under the southward IMF. However, the substorm characteristic time is about an hour for the Earth magnetosphere, and just a few minutes for the Mercury magnetosphere.

The flexibility of the paraboloid model of the magnetosphere first proposed for the Earth in [52] has allowed modifying it for other planets by adjusting particular large-scale current systems that describe magnetospheric sources or introducing new ones when necessary. The paraboloid model has the minimum number of independent input parameters, each being determined (directly or indirectly) from measurements.

The paraboloid model of the Mercury magnetosphere [96], including individual contributions from each magnetospheric current system (the planet magnetic field, the screening currents of the magnetopause, the tail current system, and the IMF penetrating the magnetosphere) succeeded in providing a good fit to measurements carried out by Mariner 10 during its first and third flybys (during the second flyby, Mariner 10 did not encounter the Mercury magnetosphere). Using these measurements and taking the just mentioned current systems into account led to improved estimates of the Mercury dipole magnetic moment, found to be equal to 192 nT R_{M}^3, and the displacement of the dipole to the north from the equatorial plane, found to be $0.18R_{\mathrm{M}}$ along the Z axis of the Mercury solar orbital (MSO) coordinate system with the origin at the Mercury center.

In computations with the paraboloid model for Mercury, R_1 was assumed to be proportional to the dynamic pressure of the solar wind to the power $-1/6$. The distance to the inner edge of the current sheet is $R_2 = 0.8R_1$, as for the Earth's tail current system. The paraboloid model enabled reproducing the structure of the Mercury magnetosphere under quiet and perturbed conditions and obtaining results well describing magnetic field measurements. Figure 7 [96] shows the pattern of the Mercury magnetic field lines computed for the noon–

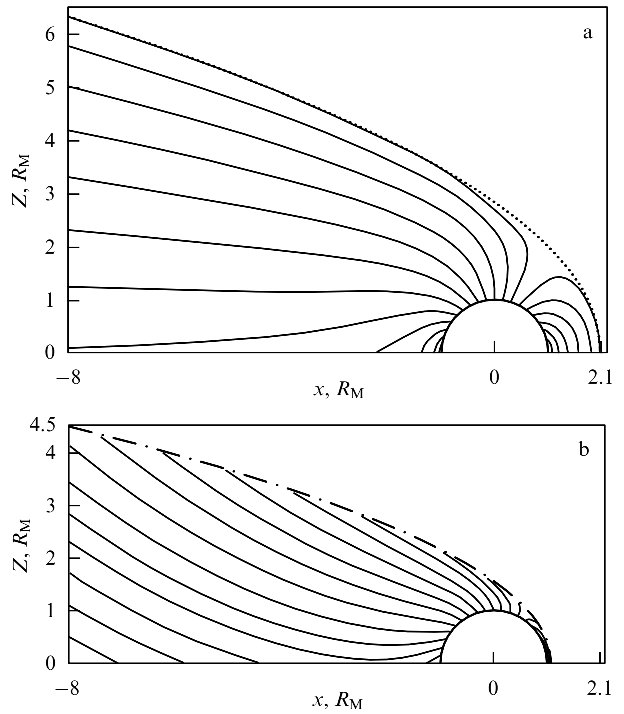

Figure 7. Magnitosphere of Mercury under quiet (a) and perturbed (b) conditions in the solar wind [96]. The magnetopause is plotted by the dotted line, and solid lines show magnetic field lines in the noon–midnight meridional section. (a) Computations were carried out for the solar wind pressure 1.3 nPa assuming the absence of the IMF penetration into the magnetosphere. The parameter of the magnetosphere found in this case is $R_1 = 2R_M$ and the radius of the polar cap found by the flux in the tail lobes is $\theta_{pc} = 37.5°$. (b) Computations for the extremely compressed magnetosphere: the solar wind pressure is ~ 84 nPa, which corresponds to $R_1 = 1.1R_M$ and $\theta_{pc} = 47°$, the IMF is 40 nT, and the magnetosphere penetration coefficien is ~ 0.4.

midnight meridian. Figure 7a presents the case of an exceptionally weak solar wind pressure. In this case, the magnetosphere of the maximum size is formed. In the case of a large solar wind pressure, shown in Fig. 7b, the magnetopause approaches the planet surface, the magnetic field on the dayside reaches 470 nT, and the neutral line in the magnetotail is located at $\sim -2.5R_M$. The computations were carried out for the southward IMF ~ 40 nT.

We briefly list other models of the Mercury magnetosphere described in Ref. [96]. In [97], a modified model of the terrestrial magnetosphere in [98] was used to explore the question of how the IMF influences the penetration of solar wind ions to Mercury. In this analytic model, the magnetopause, regarded as a cylinder on the nightside and a hemisphere on the dayside, fully screens the magnetospheric field. The IMF penetrating into the magnetosphere is added to the magnetospheric field as a perturbation, and the normal component of the magnetic field on the magnetopause remains a free parameter. The dipole tilt angle is set to zero.

Global MHD modeling [99, 100] and hybrid modeling [101–103] of the solar wind interaction with Mercury provide qualitatively similar results, especially as concerns estimates of the influence of B_z and B_x of the IMF on the topology of the day magnetosphere. In particular, all these models led to close values for the boundary of the Mercury polar cap $(45-60°)$.

A model of the Mercury magnetosphere was constructed in [104] by scaling the T89 terrestrial model in [61]. The magnetopause was only specified as a boundary of the computational domain. The tail magnetic field of the Mercury magnetosphere was modeled in [105] for the first and third flybys by Mariner 10 by scaling the Beard model [106]. The regions near the planet and in the tail were scaled separately. A scaled T96 model in [63] for the Earth magnetosphere, with the effects of B_z and B_y of the IMF taken into account, was used in [107]. This allowed modeling a perturbed magnetosphere of Mercury during the first flyby by Mariner 10, assuming that only the IMF direction was changing.

The European Space Agency is planning the project BepiColombo, which pursues the goal of exploring problems related to the origin and evolution of Mercury, and also searching for ice on the planet. Possibly, the project will include two satellites orbiting Mercury in polar orbits and one landing apparatus. One of the satellites will study the planet and the other will study the magnetosphere. Japan will participate in the development of the second satellite. The launches to Mercury are planned for 2009–2013.

4. Jupiter's magnetosphere

Jupiter is the largest planet in the Solar System and is located 5.2 AU from the Sun. Its revolution around the Sun takes 12 terrestrial years, and it rotates around its axis in about 10 h. Jupiter's equator is inclined by 3° to its orbit. 63 moons orbit Jupiter. As with most of the giant planets, the heat flux from the inner regions of Jupiter exceeds the incoming solar radiation. The Jupiter density is 1.33 g cm^{-3}; the planet is composed mainly of hydrogen (86%) and helium (14%), and does not have a rigid surface. The atmosphere of Jupiter (the most massive in the Solar System) is more than 1000 km in thickness. The pressure under it is so high that molecular hydrogen becomes liquid, and deeper, passes into a liquid-metal state. Jupiter has the strongest magnetic field, and hence the most powerful magnetosphere, continuing beyond Saturn's orbit.

Sizes of magnetospheres are commonly characterized by the distance between the planet center and the subsolar point of the magnetopause R_1. This distance is about 10 terrestrial radii for the Earth, but it is about 100 planet radii on average for Jupiter (the Jupiter radius is $R_J = 7.14 \times 10^7$ m). The polar auroras and radio emissions of Jupiter are stronger than for other planets. The Jupiter dipole magnetic moment points northward, opposite to the case of the Earth, being $|\mathbf{M}_J| \approx 4{,}2 \times 10^7$ nT R_J^3. The dipole tilt from the planet rotation axis is $\sim 9.6°$.

The Jupiter magnetic field, as well as that of other planets, has most likely occurred as a result of a hydromagnetic dynamo. It is believed that the inner part of the planet is liquid and is composed of a melt of liquid metallic hydrogen and helium. A necessary premise for the functioning of the dynamo mechanism is a geometric symmetry breaking [108]. The nonzero tilt of the dipole from the rotation axis may therefore play an essential role in the dynamo process.

The Jupiter magnetosphere is distinct from the Earth magnetosphere not only by its larger size and strength. There exist two additional factors that contribute to the difference between them: the fast rotation of Jupiter and the availability of an intense source of magnetospheric plasma, Jupiter's moon Io. Owing to vigorous volcanic activity, Io, separated by $\sim 5.9R_J$ from the planet, supplies a neutral gas to the Jupiter magnetosphere, which is abundant in sulphur, sulphur dioxide, oxygen, and sodium. The plasma composed mainly of ions of hydrogen, oxygen, and sulphur is produced from the gas released by Io as a result of ionization and recharging. Part of it forms a plasma torus in the vicinity of the Io orbit, visible even with terrestrial telescopes. The rate of plasma supply to the Io torus is estimated as ~ 1 t s^{-1} [109].

The Io plasma torus is dynamically unstable. As a result of the interchange instability, the plasma leaks from the torus (details of this process are still not fully known). In the interchange instability of the Rayleigh–Taylor type, the centrifugal force replaces the gravitational force. The resulting outward radial flow from the planet leads to plasma bending back against the rigid body rotation.

As a result of the mutual action of fast rotation and intermagnetospheric plasma production, a new source of the magnetic field, absent in the Earth's magnetosphere, emerges — the magnetodisk of Jupiter. At each field line, the centrifugal force is maximum at points of the largest separation from the rotation axis. The union of such points defines a surface located between the geographical and magnetic equator planes. One outcome is that the plasma is concentrated in the middle of the magnetosphere at low latitudes forming the magnetodisk, a thin current sheet near the equatorial plane of the magnetosphere. Its azimuthal current decreases in inverse proportion to the distance from the planet center to the power $\sim 0.8-1.7$ [110]. The total current in the disk is $\sim 10^8$ A [11, 112]. Outside the magnetodisk, the magnetic field is nearly radial and points away from Jupiter above the disk and towards Jupiter below it. In contrast to the Earth's magnetosphere, the dominant portion of energy for the Jupiter magnetosphere is supplied by the planet rotation. The effective magnetic moment of the magnetodisk exceeds the Jupiter magnetic moment by ~ 2.6 times [112].

The first direct measurements of the magnetic field in the Jupiter magnetosphere were carried out by Pioneer 10 and 11 launched in December 1973 and December 1974. It was exactly then that the Jupiter magnetodisk was discovered. Because Pioneer 10 exited the magnetosphere at 5 h 20 min LT and Pioneer 11 did so around noon at the north latitude $\sim 40^\circ$, neither satellite could detect the magnetotail of the Jupiter magnetosphere (their inbound crossing of the Jupiter magnetosphere was at dawn).

The next direct measurements of the Jupiter magnetosphere were conducted by Voyager 1 and 2. Voyager 2 was launched on 20 August 1977, and Voyager 1 slightly later, on 5 September 1977, but along a faster trajectory. Voyager 1 reached Jupiter on 5 March 1979 and Voyager 2, on 9 July 1979. Both of them detected the magnetotail of Jupiter, because Voyager 1 crossed the magnetosphere in the outbound pass at 4 h LT and Voyager 2, at 2 h 40 min LT. According to their observations, the diameter of the Jupiter magnetotail reaches $\sim 300-400R_J$ [113, 114], and it stretches beyond the Saturn orbit. In the distant magnetotail, the measured plasma density was $< 10^{-2}$ cm^{-3}, and the radial magnetic field $\leqslant 0.3$ nT. The Jupiter magnetotail, like the geomagnetic one, owes its existence to the interaction between the solar wind and the planet magnetosphere.

Voyager 1 detected a thin magnetodisk (less than 30 km in thickness) and took color images of the surfaces of Jupiter's moons it passed: Amalthea, Io, Europa, Ganymede, and Callisto. For the first time, volcanoes were observed on Io, among them at least 8 active ones. It turned out that Io is the most volcanically active celestial body in the Solar System, ejecting the hottest lava, with the temperature 1700 °C.

The trajectories of Pioneer 10 and Voyager 1 and 2 lay at low latitudes. Ulysses was launched from Cape Canaveral on 6 October 1990. In February 1992, it reached the Jupiter magnetosphere at ~ 10 h 30 min LT at the north latitude $\sim 5^\circ$ and left it at about 18 h LT at the south latitude $\sim 40^\circ$.

The Galileo orbiter launched in October 1989 began operating in the Jupiter orbit in December 1995. It passed 835 km from Ganymede, the largest moon in the Solar System, having detected its intrinsic magnetic field. Galileo then explored another Jupiter's moon, Callisto, whose surface is covered with craters. On Europa, a moon covered with ice, multiple ice cracks were discovered. It was hypothesized that salty water may exist below the ice, conceivably hosting primitive forms of life. Similar oceans possibly exist beneath the ice crust on Ganymede and Callisto. Galileo also explored polar auroras on Io and Jupiter, and Io's torus. In September 2003, having completed the 35th loop around Jupiter, Galileo was destroyed by being sent into the Jupiter atmosphere.

The Cassini spacecraft was launched in 1997 toward Saturn and reached it on 1 July 2004. The interplanetary flight of Cassini included flybys of Venus, Earth, and Jupiter. It intersected the Jupiter orbit on 30 December 2000, moving approximately tangent to the bow shock and the magnetopause. The influence of solar wind parameters on the location of these surfaces was observed.

One more space mission, New Horizons, launched on 19 February 2006, approached Jupiter in February 2007 during minimum solar activity and explored the nightside of Jupiter, in particular, auroras and the magnetotail. In addition, data on the evolution of ammonium clouds in Jupiter's atmosphere were collected. Currently, New Horizons has already passed the Saturn orbit. Exploring Pluto and its moon Charon is scheduled with its assistance for 2015, and the Kuiper belt, for 2016–2020.

In contrast to the data obtained by Voyager, Ulysses discovered large-scale anticorotational streams of plasma [115–118] in the external low-latitude Jupiter magnetosphere in the vicinity of the noon meridian. During the first pass of Ulysses through the boundary of the Jupiter magnetosphere, the magnetic field on both sides of the magnetopause was approximately equal. Consequently, the plasma pressures in the solar wind and magnetosphere had to be equal as well (the Earth's magnetospheric plasma is much more rarefied than the interplanetary one). For Jupiter, a significant contribution to the pressure balance comes from heavy ions originating from neutrals released by Io. Moreover, the Jupiter magnetospheric plasma is formed through the ionization of neutral atoms of the Jupiter atmosphere, neutral particles from tori linked to other moons, and a neutral interstellar medium with a negligibly small density. Measurements show that the main contribution comes from Io. Hence, the distance to the subsolar point of the Jupiter magnetopause is influenced not only by the dynamic pressure and magnetic field of the solar wind but also by the state of Io's volcanic activity. The presence of the dayside Jupiter magnetopause was observed at distances $50-150R_J$ [119].

Jupiter is a rapidly rotating planet with a strong magnetic field. Its atmosphere transfers angular momentum from the planet surface to the ionosphere, where the plasma undergoes a transition to a corotation regime due to collisions with

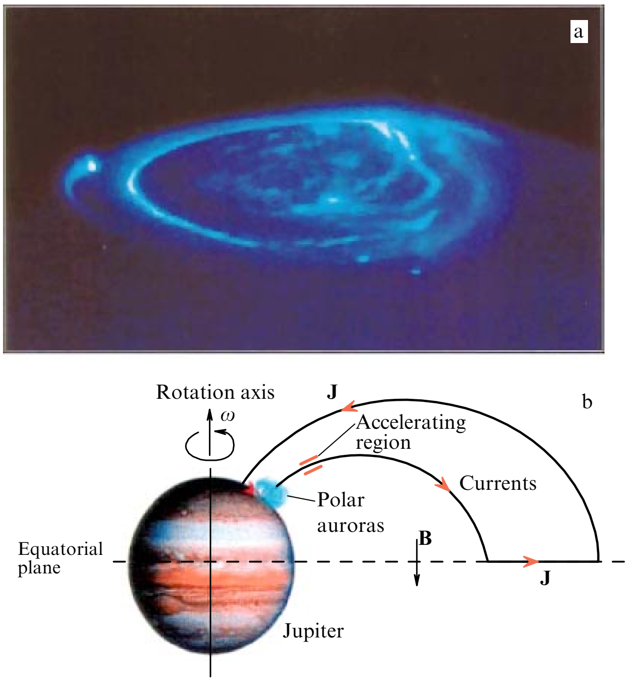

Figure 8. Image of polar aurora on Jupiter in the ultraviolet band observed by the Hubble Space Telescope [122]. (b) Schematic of the electric circuit involved in polar aurora generation on Jupiter (see Ref. [73]).

neutrals. In the approximation of rigid-body rotation, the electric field of corotation is defined as

$$\mathbf{E}_{\rm cor} = -[\mathbf{\Omega}_{\rm J} \times \mathbf{r}] \times \mathbf{B}\,, \tag{4}$$

where $\mathbf{B}$ is the magnetic field, $\mathbf{r}$ is the radius vector drawn from the Jupiter center, and $\mathbf{\Omega}_{\rm J} \approx 1.76 \times 10^{-4}$ s^{-1} is the Jupiter angular rotation speed. The electric field of corotation is transferred to the magnetosphere under the assumption that the magnetic field lines are equipotential. The electric corotation field is directed from Jupiter in the magnetic equator plane, its magnitude reaching $E_{\rm r} = 5.3(R_{\rm J}/L)^2$ V m^{-1}, where L is the distance from the Jupiter center in the equatorial plane expressed in Jupiter radii. For a rigid corotation, the velocity is $V_{\rm rigid} = 12.6L$ km s^{-1}.

Jupiter's polar auroras have been explored both in the ultraviolet band with the Hubble Space Telescope and in the infrared band with ground-based telescopes [120]. These auroras are characterized by persistently present and relatively stable auroral ovals surrounding the north and south poles and projecting along closed magnetic field lines into the middle magnetosphere (to distances $\geqslant 20-30R_{\rm J}$). The light of the ovals is attributed to the precipitation of electrons with mean energies 5–150 keV. Based on the Doppler shift of the H_3^+ line of ionospheric ions, it was established that the ovals are related to the magnetospheric plasma lagging behind the rigid corotation [121].

Figure 8a presents the structure of Jupiter's polar auroras as observed by the Hubble Space Telescope in the ultraviolet range [122]. The polar auroras of Jupiter include (in the order of increasing latitude) (1) the emission caused by moons Io, Europa, and Ganymede; (2) the narrow bright main auroral ovals at the colatitude $15-16°$; and (3) a varying glow of polar caps bounded by the main ovals on the equatorial side.

In [123], the main auroral ovals of Jupiter were interpreted as ionospheric roots of outflowing field-aligned currents related to a partial corotation of the magnetospheric plasma moving from its source (the plasma torus of Io) to the outer magnetosphere, and from there to the solar wind. The transfer of angular momentum outside Jupiter requires that the ionospheric current be directed toward the equator and, in the plane of the magnetospheric equator, radially from the planet. The field-aligned currents closing these transverse currents are directed from Jupiter at low latitudes and toward it at high latitudes. A simplified schematic of such a current system is shown in Fig. 8b [73]. It is commonly conjectured that outflowing currents are carried by magnetospheric electrons passing through an accelerating gap. An accelerating gap with a finite potential difference across it emerges when the magnitude of the field-aligned current exceeds some threshold value determined, for example, by the density of charge carriers. Affected by a finite potential difference, the electrons are accelerated down to the ionosphere.

A decrease in the azimuthal velocity by 20–30% with respect to the rigid corotation was observed at equatorial distances $\sim 20R_{\rm J}$ from the planet center [124]. This is related to radial outflow of plasma from the Io torus, preserving the angular momentum. Correspondingly, the field-aligned currents have to be confined to field lines passing through this region. Because just this region is mapped to auroral ovals, it can be argued that they correspond to braking zones of corotating magnetospheric plasma. Hence, Jupiter's rotation serves as an energy source for the emission of the main polar ovals. In the case of the Earth, the energy of the polar aurora emission is eventually provided by the solar wind.

A lagging of the plasma in the low-latitude Jupiter magnetosphere behind the rigid corotation was observed by Pioneer 10 and 11, Voyager 1 and 2, Ulysses, and Galileo. It reached $\sim 50\%$ in the middle magnetosphere and increased even more toward the external magnetosphere. At locations where the plasma outward motion defines the magnitude and configuration of the magnetic field (in particular, in the magnetodisk), the lagging of the rigid corotation is well pronounced.

The effective braking of angular rotation caused by the outward radial motion of the plasma in the low-latitude magnetosphere is transferred to the ionosphere along highly conductive magnetic field lines. This leads to braking of the rigid corotation in the ionosphere. The rigid corotation determines the electric potential

$$U_{\rm rig} = B_{0\rm J}\Omega_{\rm J} R_{\rm J}^2 \sin^2\vartheta\,, \tag{5}$$

where $B_{0\rm J}$ is the field at the Jupiter equator and ϑ is the colatitude. At the level of the ionosphere, the electric potential of corotation, corrected with regard to the differential rotation in the equatorial magnetosphere, is expressed as [112]

$$U_{\rm cor} = B_{0\rm J}\gamma\Omega_{\rm J} R_{\rm J}^2 \sin^2\vartheta + C\,, \tag{6}$$

where γ and C are constants determined from observations and dependent on the equatorial distance of the magnetic field line whose ionospheric foot is at the polar angle ϑ from the Jupiter center. The constant C ensures the continuity of the potential across the boundaries with different rotation regimes (different γ, where $\Omega = \gamma\Omega_{\rm J}$ is the effective angular rotation speed). We assume that $U_{\rm cor} = 0$ where the rotation is absent. It follows from Eqn (6) that latitude lines are simultaneously equipotential lines of the electric field of rotation.

Observations by Pioneer 10 provided evidence [119] of the availability of open field lines along which energetic particles escape from the Jupiter magnetosphere. Hence, although Jupiter has a strong intrinsic magnetic field and an even stronger field of the magnetodisk, located approximately 18 to $92 R_J$ [125] (the distance to the outer edge of the magnetodisk varies as a function of R_1), the weak IMF that penetrates into the magnetosphere essentially impacts the topology of the Jupiter magnetospheric field.

In the paraboloid model of the Jupiter magnetosphere, the magnetopause is modeled by a paraboloid of revolution. This model includes the Jupiter dipole magnetic field and the magnetic field of the magnetopause currents that screen it, the magnetic field of the magnetotail (transverse currents and their closure at the magnetopause), and the magnetic field of the magnetodisk and that of the currents screening it. In the paraboloid model, the boundary conditions at the magnetopause for partially penetrating magnetic and electric fields of the solar wind were taken in the forms $\mathbf{b} = k_J \mathbf{B}_{\mathrm{IMF}}$ and $\mathbf{E} = k_J \mathbf{E}_{\mathrm{IMF}}$, where k_J is the penetration coefficient, and $\mathbf{B}_{\mathrm{IMF}}$ and $\mathbf{E}_{\mathrm{IMF}}$ are the unperturbed interplanetary magnetic and electric fields. Along highly conducting magnetic field lines, the electric potential can be mapped from the magnetopause to the magnetosphere. The Jupiter magnetic disk has no analogs in the Earth's magnetosphere; its modeling is carefully described in Refs [112, 126, 127].

Results of computations of the Jupiter magnetosphere structure performed with the paraboloid model are shown in Fig. 9a, b [112] for the southward and northward IMF. For $B_{\mathrm{IMF}y} = 0$, the electric potential created by the MHD solar wind generator is $U_{\mathrm{sw}} = y k_J V_{\mathrm{sw}} B_{\mathrm{IMF}z} R_J$. The value of the penetration coefficient for the IMF may be higher for the Jupiter magnetosphere than for the Earth's magnetosphere; k_J can approach unity [112]. Therefore, electric equipotentials $U_{\mathrm{sw}} = \mathrm{const}$ coincide with $y = \mathrm{const}$ lines. The northward IMF for Jupiter is analogous to the southward one for the Earth, and vice versa. For the southward IMF, the reconnection occurs at the neutral points of the magnetic field in the vicinity of the cusps (Fig. 9a), and for the northward, at quasineutral line located at the dayside low-latitude magnetopause and in the current sheet of the magnetotail (Fig. 9a). The pattern is similar to that obtained by Dungey for the Earth for a strong southward IMF. The difference is brought about by the fast rotation of the powerful magnetic field of Jupiter. It follows from Fig. 9 that even a small fraction of the IMF penetrating into the Jupiter magnetosphere ($b = 0.03$ nT) has an appreciable impact on the structure of the magnetospheric magnetic field.

Figure 9c presents results of computing the electric and magnetic fields in the paraboloid model of the Jupiter magnetosphere for the northward IMF with $k_J = 1$: $B_{\mathrm{IMF}x} = -0.02$ nT, $B_{\mathrm{IMF}y} = 0$ nT, and $B_{\mathrm{IMF}z} = 0.5$ nT [112]. Solid lines show electric equipotentials of corotation, forming vortices in the equatorial plane of the magnetosphere and in the magnetopause. The dot-dashed lines correspond to equipotentials of the electric field generated by the solar wind. In the tail lobes, the rigid corotation is likely to persists up to the distances where the corotation speed becomes comparable to the Alfvén speed (inside the Alfvén radius), under the condition that the magnetic field lines are equipotential. Beyond the Alfvén radius, information about the rigid corotation cannot propagate with the Alfvén speed along the magnetic field lines. The Alfvén speed in the lobes of the Jupiter magnetotail is much higher than in the equatorial plane, reaching $\sim 31 \times 10^3$ km s^{-1} [128, 129], because the plasma density there is $\sim 10^{-5}$ cm^{-3}. In this approximation, the Alfvén radius in the tail lobes is $\sim 2.5 \times 10^3 R_J$. It therefore follows that for the northward IMF, the rigid corotation can be transferred along open magnetic field lines as far as the magnetopause [112]. If the equipotentiality of the magnetic field lines is violated, there is lagging against the rigid corotation on open field lines for the northward IMF.

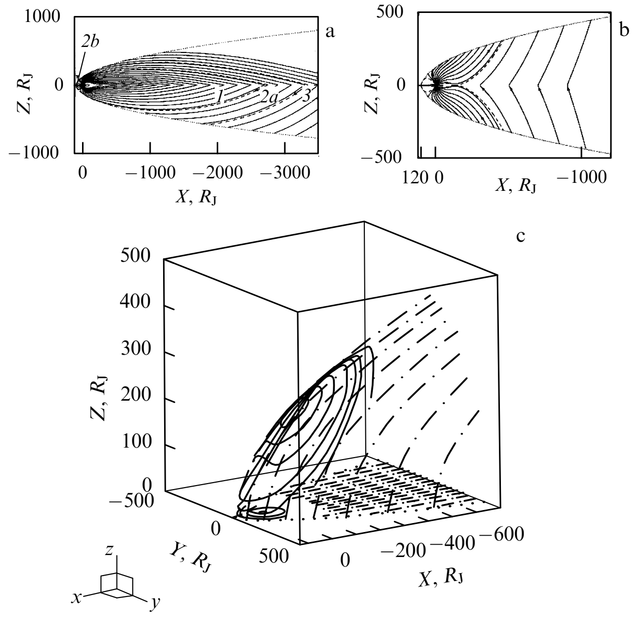

Figure 9. The magnetosphere of Jupiter computed in the framework of the paraboloid model. Shown are magnetic field lines in the meridional noon–midnight section of the open model of the Jupiter magnetosphere for southward (a) and northward (b) IMF. The IMF components in the Jupiter solar–magnetospheric system of coordinates: $B_{\mathrm{IMF}x} = -0.26$ nT, $B_{\mathrm{IMF}y} = 0$ nT, $B_{\mathrm{IMF}z} = -0.2$ nT, and $k_J = 0.1$ (a); $B_{\mathrm{IMF}x} = -0.02$ nT, $B_{\mathrm{IMF}y} = 0$ nT, $B_{\mathrm{IMF}z} = 0.5$ nT, and $k_J = 1$ (b). The dashed curves separate magnetic field lines of different topological types: *1* — closed field lines, *2a* and *2b* — open field lines of southern and northern polar caps; *3* — interplanetary field lines that reached the magnetosphere [112]. (c) The three-dimensional Jupiter magnetosphere for the northward IMF. The IMF components penetrated the magnetosphere in Jupiter's solar–magnetospheric coordinate system: $B_{\mathrm{IMF}x} = -0.02$ nT, $B_{\mathrm{IMF}y} = 0$ nT, $B_{\mathrm{IMF}z} = 0.5$ nT. Digits near the lines of the northern latitude (solid lines) indicate the latitude in degrees; those near lines $y = \mathrm{const}$ on the magnetopause (dash-dotted lines) correspond to y expressed in Jupiter radii [112].

Anticorotational streams directed from the Sun, observed by Ulysses in the dawn–noon sector for the southward IMF in the equatorial magnetosphere of Jupiter and on the lines connected to the polar caps, agree well with computations performed with the paraboloid model, which accounts for the braking of rotation of the low-latitude magnetospheric plasma and the penetration of the solar wind magnetic field into the magnetosphere. The presence of such streams during the Ulysses flyby and their absence for flybys by Pioneer 10 and Voyagers 1 and 2 is attributed to the different orientation of the north–south component of the IMF in these cases. For the northward IMF, model computations demonstrate the prevalence of corotation and the absence of anticorotational streams in the noon- and dawnside equatorial magnetosphere of Jupiter, and motion in the anti-sunward direction in the magnetotail behind the neutral line [112]. These findings agree well with data from Pioneer 10 and the Voyagers, which observed, for the northward IMF, corotation in the equatorial magnetosphere of Jupiter preserved until the subsolar magnetopause and motion in the anti-sunward direction in the magnetotail for $r > 150R_{\mathrm{J}}$ (the so-called 'magnetospheric wind').

We list some currently existing models of the Jupiter magnetosphere. These include the models by Hill et al. [130], Barish and Smith [131], Smith et al. [132], Beard and Jackson [133], Goertz [134–136], Engle and Beard [137], Acuña et al. [138], Connerney et al. [139, 140], and Khurana [141]. Most of them describe observational data obtained during rare flybys of spacecraft through particular regions of the Jupiter magnetosphere. The contribution of the IMF to the interaction of the solar wind with the magnetosphere was not taken into account. In contrast to the majority of the existing models, the paraboloid model of the Jupiter magnetosphere is applicable not only in the equatorial plane near the planet but also in high latitudes and the outer magnetosphere. Moreover, this is the only analytic model that considers the influence of the IMF.

In the model in [141], an expansion in spherical harmonics was used, as in the O6 model [142], to compute the internal field, and the external field was computed by Euler potentials. In particular, the magnetic field of the current disk was modeled with the help of the Euler potential used in Ref. [143]. The model in [141] takes the complex form and geometry of the Jupiter magnetodisk into account, as well as the realistic profile of the azimuthal current density there. For radial distances greater than $\sim 30R_{\mathrm{J}}$, the magnetodisk was aligned with the magnetic equator plane departing further toward the geographical equator. Such behavior of the magnetodisk corresponds to observations and is explained by the outward plasma motion, its lagging against the rigid corotation, and the angular momentum conservation. The deviation of the field lines from the meridional plane related to the radial currents was also computed.

The model in [140] assumes an axial symmetry of the magnetospheric field, including the magnetodisk. The planetary magnetic field is expanded in spherical harmonics using direct measurements of the magnetic field. The field of the magnetodisk was modeled by fitting the data of the Voyager mission. A three-dimensional current system connected with the main auroral ovals of Jupiter was described in [123]. In [144], based on observations from Cassini and Galileo, the influence of the IMF on the Jupiter magnetosphere was investigated. The position of the magnetopause and the bow shock varied together with the north–south component of the IMF. The three-dimensional MHD modeling of the interaction of solar wind with the Jupiter magnetosphere was used in [145].

Observations by the Voyagers, Ulysses, Galileo, Wind, and Cassini have demonstrated that all planets having an intrinsic magnetic field, especially the outer planets, emit intense nonthermal radiation [146]. The radio frequency emission of the outer planets originates in the auroral regions and radiation belts, and is also modulated by some moons. Electrons of the Jupiter radiation belts are the source of synchrotron radiation in the decimeter range [147].

In 1955, a powerful emission from Jupiter in the dekameter range was discovered [148]. It was soon associated with the cyclotron emission of electrons, being the first clue to the existence of the Jupiter magnetic field. Subsequently, models based on the cyclotron instability were proposed for the emission generation. Presently, it is supposed that the auroral and coherent radio emission induced by Jupiter's moons is rooted in a cyclotron maser instability, while the radiation belts serve as sources of noncoherent synchrotron radio emission [149]. Amplification and excitation of the maser cyclotron instability emission is linked to a non-equilibrium electron distribution over velocities, which is analogous to the inverse population of maser energy levels, and leads, on relaxation, to fast, coherent emission [150].

It is assumed that emission in the middle and high-frequency ranges of the planetary radio spectrum (from several kHz to several MHz) is generated by a cyclotron maser instability in the field lines linked to auroral activity in the vicinity of the planet. This hectodecameter radio emission from Jupiter is 10^5 times stronger than the emission from the radiation belts [146]. The field-aligned currents related to the polar oval appear due to violation of the rigid corotation for Jupiter. The sources of hecto- and decameter emission are therefore present for all local times. The auroral radio emission from Jupiter is generated along high-latitude magnetic field lines by accelerated electrons causing polar auroras [151]. It was discovered that the emission in the hectometer range varies together with the polar auroras. Simultaneous observations of hectometer emission and polar auroras on Jupiter in the extra-ultraviolet range using Cassini and Galileo indicated that the arrival of interplanetary shock waves from the Sun triggers intensification of emission of these two types. An arrival of a shock wave on Jupiter is accompanied by compression and rearrangement of the Jupiter magnetosphere, which results in excitation of electric fields and acceleration of electrons along auroral field lines [151].

The radio emission of Jupiter has been continuously monitored for the last decade with the help of space and ground-based measurements [152]. The Galileo probe studied the emission in the kilometer and hectometer ranges; and Wind and ground-based telescopes, in the hectometer and decameter ranges. In combination with ground-based measurements, particular configurations were used between Cassini approaching Jupiter and Wind flying around the Earth, and between Galileo orbiting Jupiter and Wind. This made the radiotomography of Jupiter possible [152].

Decameter emission from Jupiter has a sporadic character, i.e., is composed of separate bursts of variable intensity. Despite this, the emission shows features that point to relations to a stable magnetic configuration [150]. Using ground-based measurements of the decameter emission of Jupiter, which correlates with the longitude of its central meridian, the planet rotation period was determined. It was also discovered that the decameter emission intensity increases in some active regions of Jupiter. It was possible to separate the decameter emission from Jupiter that is controlled by Io. As Jupiter's magnetospheric plasma flows past Io, the Alfvén wings that connect Io with the Jupiter ionosphere in the northern and southern hemispheres are excited. The maximum current in the Alfvén wings is of the order of 10^8 A. The induced electric field accelerates electrons, contributing to the decameter emission generation [150].

Specific aspects of the Jupiter radio emission linked to Io and its plasma torus were studied, in particular, in Refs [153, 154]. Statistical analysis of the decameter emission of Jupiter modulated by Io demonstrated that it depends on the longitude of the Jupiter central meridian. This is because there exist 'active' longitudes of Io — its particular positions in the orbit that are fixed with respect to the Jupiter magnetic field and at which the emission related to Io occurs most frequently. The mechanism explaining the emergence of 'active' longitudes for Io was discussed in Refs [153, 154]. It is determined by two factors: first, the modulation of the particle acceleration efficiency in the Io ionosphere as it moves in the inhomogeneous magnetic field of Jupiter, and second, the scattering over the pitch-angle of accelerated electrons in the Io plasma torus. This mechanism enabled explaining the preferred localization of emission sources in the northern hemisphere of Jupiter [154].

The motion of Io in the Jupiter magnetic field can lead to the acceleration of electrons in the Io ionosphere [153]. As Io orbits, an electric field $\mathbf{E}_i$ perpendicular to the magnetic field is induced in its ionosphere. However, owing to the anisotropic conductivity of the Io ionosphere, there arise Pedersen (along $\mathbf{E}_i$) and Hall (perpendicular to the electric and magnetic field, and also to Io's surface) currents. Because of the nonconducting atmosphere, the Hall current is not closed, which entails charge separation in the ionosphere. The electric field associated with charge separation has the projection along the magnetic field of a magnitude comparable to $\mathbf{E}_i$. This projection accelerates electrons. In addition to the electric field effect, fast electrons gain speeds in excess of the thermal one on collisions with atoms. This leads to the excitation of the Buneman instability and additional heating of the electrons. The consequence is that electrons escape along the magnetic field. Typical energies and streams of accelerated electrons in the field tube of Io have been estimated. The energy stored in the electron stream is sufficient to sustain the electromagnetic radiation of the Io magnetic field tubes [153].

Thus, part of the decameter emission from Jupiter is modulated by its moon Io, which induces additional precipitation of electrons in the magnetic tube connecting Io with Jupiter. Moreover, as follows from measurements conducted by Galileo and Voyager 1 and 2, the radio emission from Jupiter is also influenced by Callisto and Ganymede.

In July 1994, an exclusive rare event occurred — the collision of the Shoemaker–Levy 9 comet with Jupiter. The comet consisted of 25 luminous objects stretched into a chain several million kilometers in length, supposedly the debris of a single celestial body. According to computations of its trajectory, this body already flew by Jupiter in June 1992 and was torn apart by Jupiter's tidal forces caused by the gradient of the Jupiter gravitational field [155]. The collision was accompanied with a wealth of effects in the atmosphere, ionosphere, and magnetosphere of Jupiter. The collision process was followed by almost all large world observatories, the Hubble space telescope, and the Ulysses and Voyager spacecraft. Bursts of emission caused by collisions of comet debris were recorded in a broad spectral range. The collision triggered vigorous gas ejections. Large-scale long-lived vortices formed in the atmosphere of Jupiter. As the comet fragments fell, a brightening of Jupiter's radiation belts in the decimeter range, the generation of artificial auroras in both hemispheres, a weakening in brightness of the Io plasma torus in the extra-UV range, and other phenomena were observed. Review [155] collects the observational data and proposes a physical model that plausibly explains them.

It is noteworthy that most of the measurements in the Jupiter magnetosphere, including those provided through the Voyager and Galileo missions, were carried out in the vicinity of the equatorial plane, except portions of the trajectories of Pioneer 11 and Ulysses before the outbound crossing of the magnetosphere at middle latitudes. The first polar observations of auroral plasma and Jupiter fields are planned for the future NASA mission Juno [120]. Juno is scheduled to leave the Earth in August 2011 and, having reached Jupiter, to become its polar orbiter beginning from 2016, rotating from pole to pole on a low elliptic orbit. Juno will measure the gravitational and magnetic fields of Jupiter and study the structure of its atmosphere and the internal composition. To explore the origin of Jupiter, Juno will measure the total oxygen and nitrogen content. It will be the first spacecraft to probe the structure and dynamics of the Jupiter atmosphere below the cloud layer. Data on the Jupiter Great Red Spot, a particular cyclone persisting for hundreds of years, will be collected. The nature of the Jupiter polar auroras, the most powerful ones in the Solar System, will be investigated. The energy supply of Juno will be provided by solar cells. Because Jupiter is 5.2 times farther from the Sun than the Earth, Juno will collect 3.7% of the energy it would have collected were it orbiting the Earth. The Juno trajectory is computed so as to avoid passing through the Jupiter radiation belts, which are denser than the Earth's radiation belts.

One more future project called Laplace is planned for 2015 to 2025 by Russian and European scientists. The project goal is to search for the simplest life forms on Jupiter's moon Europa. The main task of the project is to explore the surface of Europa on which, supposedly, an ocean of water is confined beneath the ice layer. A landing robot is planned for drilling the surface ice and taking probes from deeper layers.

5. Saturn's magnetosphere

Saturn is 9.58 AU from the Sun. It is composed of liquid hydrogen and helium and is surrounded by a prominent system of rings and numerous moons (currently, 56 are known), the largest being Titan, with the radius 5150 km. Saturn revolves around the Sun in an almost circular orbit with the period of 29.5 terrestrial years. The inclination to the ecliptic is 2°, whereas the equatorial plane of Saturn is inclined by 27° to its orbital plane, which is responsible for a seasonal cycle. The radius of Saturn is $R_S = 60{,}268$ km. Its rotation period is 10 h 40 min. The atmosphere is composed of 94% hydrogen and 6% helium. The heat flux from the interior of Saturn exceeds the solar heat flux, similarly to Jupiter. Saturn has a strong magnetic field with the dipole moment pointing northward and being equal to 0.21 G R_p^3; the magnetic dipole axis coincides with the planet rotation axis (for the Earth and Jupiter, the axis is tilted at $\sim 10°$ to the rotation axis) and is slightly displaced along the polar axis (by $0.04 \pm 0.02 R_S$ [156]). The internal field of Saturn can be represented in terms of dipole, quadrupole, and octupole terms. Its octupole term is considerably smaller than those for the Earth and Jupiter.

The first spacecraft to explore Saturn was Pioneer 11. Launched on 15 April 1973, it reached the closest distance to the planet on 1 September 1979. Voyager 1 and 2 were the next spacecraft to pass through the Saturn magnetosphere. Voyager 1 approached Saturn as close as 124,000 km on 12 November 1980. With its assistance, images of many of Saturn's moons were obtained. It was found that most of them are composed of water ice. On 12 October 1980, Voyager passed 4000 km over the surface of the largest moon of Saturn, Titan. The image obtained by it shows a thick atmosphere composed by 98% nitrogen and almost fully covering Titan's surface. Voyager 2 approached closest to Saturn on 26 August 1981. The Pioneer 11 and Voyager 1 and 2 spacecraft entered the Saturn magnetosphere near noon and left it at dawn. The Cassini spacecraft, launched in 1997, encountered Saturn on 1 July 2004 and has become its orbiter. By the end of the first revolution, it released the Huygens probe that descended to Titan to explore its atmosphere.

The magnetosphere of Saturn is intermediate between those of the Earth and Jupiter. The distance to the subsolar point of the Saturn magnetopause is $R_1 = 17-24R_S$. The plasma in the saturnian magnetosphere is driven by the planet rotation and the solar wind. The electric field of corotation prevails over that of convection, generated by the solar wind, to radial distances $21R_S$ [156]. The rigid corotation persists to $10R_S$ (in the Earth's case, it ends at $6R_E$); further, the rotation proceeds at the angular speed $\sim 0.3-0.8$ of the rigid corotation speed. Pioneer 11 has discovered an elongated magnetotail of the Saturn magnetosphere.

The distance to the subsolar point R_1 depends on the solar wind pressure. During the flyby by Pioneer 11, the fast solar wind ($V_{sw} = 470$ km s^{-1}) forced the compression of the magnetosphere to $R_1 = 17R_S$. During the flyby by Voyager 2, the solar wind was less perturbed and $R_1 = 19R_S$. The flyby by Voyager 1 occurred for a quiet solar wind and $R_1 = 23-24R_S$. An even less dense and slower solar wind was detected during the first revolution of Cassini around Saturn; in that case, $R_1 = 28R_S$.

The fast rotation of Saturn and the presence of the magnetospheric plasma enforce a relatively strong ring current — a downscaled analog of the Jupiter magnetodisk. In contrast to Jupiter, for which the main source of the magnetospheric plasma is its moon Io, the sources of the Saturn magnetospheric plasma are icy moons and rings, and the atmospheres of Saturn and Titan. The total integrated ring current is $\sim 10^7$ A. The spatial localization of the ring current was determined from the data of the Pioneer 11, Voyager 1 and 2, and Cassini spacecraft [157–159]. It turned out that the inner and outer edges of the ring current, confined within the equatorial magnetosphere, as well as its thickness, vary with time. As the size of the system (R_1) increases with decreasing the dynamic pressure of the solar wind, the distances to the edges of the ring current, the current magnitude, and its magnetic moment also increase. It is assumed that this happens as a consequence of the balance of radial tensions in the plasma in a rapidly rotating magnetosphere [159].

The polar auroras on Saturn are located closer to the poles (at the colatitude $10-15°$) than on Jupiter ($16°$) [160]. The near-pole boundary of the auroral oval of Saturn lies near the expected boundary between open and closed field lines [161]. The ovals of polar emissions on Saturn are not linked to the braking of the rigid corotation as on Jupiter, but are related to currents connecting the magnetosphere with the solar wind, as on the Earth [160]. It was mentioned in [162] that polar auroras on Saturn vary slowly, some elements being involved in corotation and some not, which possibly hints at their relation to the solar wind. The polar auroras on Saturn reflect variations in the structure and magnetic field of the solar wind [163–166]. During storms in the Saturn magnetosphere, generated by the solar wind, the intensity of oval emissions increases mainly in the dawn sector [167].

While the speed of the solar wind is virtually independent of the distance, the plasma density decreases from ~ 5 cm^{-3} at the Earth's orbit to ~ 0.03 cm^{-3} at Saturn's, and the magnitude of the IMF decreases in inverse proportion to the distance to the Sun. Therefore, the IMF in the Saturn orbit (~ 0.3 nT) is approximately an order of magnitude lower than for the Earth (~ 5 nT). Furthermore, the mean angle at which the IMF is oriented to the orbit, following the Archimedes spiral, also varies. Nevertheless, under the appropriate conditions, the magnetic and electric fields of the solar wind formidably change the structure of the Saturn magnetosphere, which, in particular, is reflected in polar auroras [164–166, 168]. This happens mainly when strong perturbations in the solar wind arise.

Direct evidence of the dependence of UV auroras on Saturn on the solar wind was first obtained during joint observations performed by the Cassini spacecraft and the Hubble Space Telescope in January 2004, when Cassini was upstream from Saturn. During the Cassini flyby, in the decay phase of the solar cycle, the interplanetary medium in the Saturn orbit was structured by corotating interaction regions (CIRs) [169]. The solar wind was composed of alternating zones with a large magnetic field and high pressure, so-called compression zones, and those with low pressure and a weak field, the rarefication zones. The duration of these zones reached several days. The magnetic field reached 0.5–2 nT in the compression zones of the solar wind, and was $\leqslant 1$ nT in the rarefication zones.

Images obtained at this time by the Hubble Space Telescope are reproduced in Fig. 10a. The rarefication zones in the solar wind are associated with an expanded oval, and the compression zones, with a contracted one [161, 163]. Under the assumption that the subpolar boundary of saturnian auroras coincides with that of the open field line region, it turns out that the abrupt decrease in the flux of open field lines is related to conditions in the interplanetary space — the arrival of compression zones of the solar wind.

The paraboloid model of the Saturn magnetosphere was constructed to describe global magnetospheric current systems and account for the interaction with the solar wind and its magnetic field [158, 159, 164–166]. The model includes the intrinsic dipole magnetic field, the ring current field, the magnetotail current system, and currents at the magnetopause that shield magnetospheric field sources. Additionally, the IMF penetrating the magnetosphere is taken into account. Each current system is included in the model as an independent block.

Figure 10b presents the meridional noon–midnight section of the Saturn magnetosphere. Computations were carried out with the paraboloid model based on parameters derived from the data collected by Pioneer 11 on entering the magnetosphere [158]. The broken line in Fig. 10c (black in the electronic version) plots, on a logarithmic scale, the modulus of the magnetic field measured by Pioneer 10 as it crossed the magnetosphere of Saturn on the inbound pass. The position of the magnetopause (MP) and the point of closest approach to Saturn (CA) are marked with vertical dashed lines. The abscissa presents day of the year (DOY) and the respective distance to the planet center expressed in R_S. The lower line (blue in the electronic version) plots the modulus of the magnetic field computed with the SPV model — the best model describing the magnetic field up to $8R_S$, designed by combined data collected by Pioneer 11

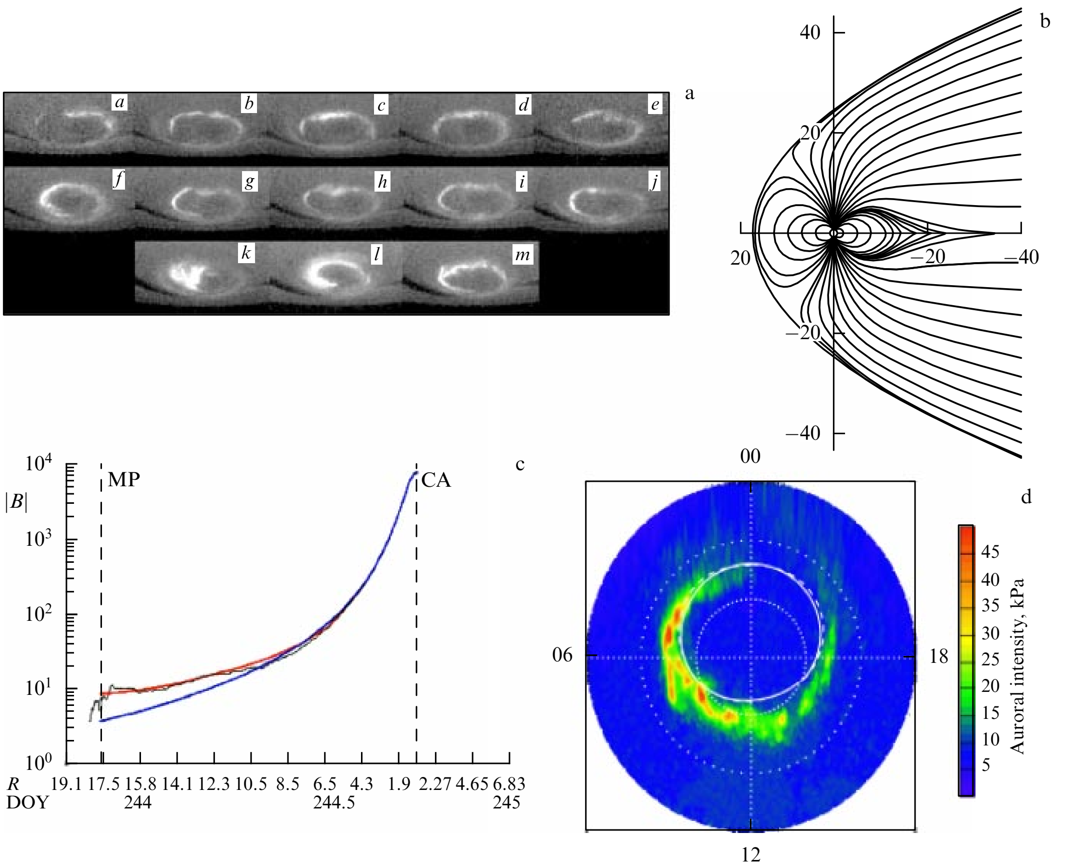

Figure 10. (a) UV images of polar auroras on Saturn in the southern polar cap obtained with the Hubble Space Telescope on 8, 10, 12, 14, 16, 18, 20, 21, 23, 24, 26, 28, and 30 January 2004, marked with letters from a to m [161, 163]. Noon is at the top, dawn is to the left. The dark arch in the bottom portion of each image corresponds to the southern polar limb of the planet. (b) Meridional noon–midnight section of the Saturn magnetosphere. The computations were carried out in the framework of the paraboloid model with parameters retrieved from data obtained by Pioneer 11 during inbound crossing of the magnetosphere [158]. (c) The irregular curve (black in the electronic version) shows, on a logarithmic scale, the modulus of the magnetic field registered by Pioneer 11 during its inbound pass through the magnetosphere. The modulus of the magnetic field computed with the SPV model is displayed by the lower curve (blue in the electronic version). The result of computations performed using the paraboloid model is presented by the smoother curve (red in the electronic version). MP and CA mark the magnetopause and the closest approach to Saturn. The abscissa shows numbers of days in a year (DOY) and the corresponding distance from the center of the planet expressed in its radii [158]. (d) Comparison of polar auroras in the southern polar cap of Saturn with computations in the framework of the paraboloid model (white curves) for the image obtained on 30 January 2004. The solid line corresponds to the dynamic solar wind pressure 0.03 nPa, and the dotted one, to 0.08 nPa [166]. The penetration coefficient of the IMF $(-0.3, 0.7, 0.7)$ nT was chosen equal to 0.2.

and Voyager 1 and 2 [170]. The smoother curve (red in the electronic version) plots the result delivered by the paraboloid model of Saturn using the parameters determined in Ref. [158]. The computed field agrees with observations over the whole portion of the Pioneer 10 trajectory as it was approaching Saturn, in contrast to the SPV model, which is well suited only at very close separations $< 4R_{\rm S}$.

Figure 10d presents a comparison of the Saturn polar aurora pattern obtained with the Hubble Space Telescope on 30 January 2009 with computation of the boundary of open field lines in the paraboloid model of the magnetosphere for the northward IMF with the components $(-0.3, 0.7, 0.7)$ nT measured by Cassini [166]. In the computations, the coefficient of IMF penetration into the Saturn magnetosphere was chosen as ~ 0.2. The white curves plot the results of model computations with the solar wind dynamic pressure 0.03 nPa (the solid line) and 0.08 nPa (the dashed line). The boundary of open field lines closely follows the poleward boundary of the Saturn oval of polar auroras.

The paraboloid model is currently the only one providing the global magnetic field of Saturn that agrees well with observations. The other available models describe the sources of the magnetospheric field only partially. For example, a model for the ring current in the Saturn magnetosphere based on Voyager 1 and 2 data was proposed in [171]. This model was subsequently generalized in [172] using data provided by Pioneer 11. A model of the Saturn magnetosphere proposed in [173] includes currents at the magnetopause, but lacks magnetotail currents whose magnetic field is of particular importance on the nightside of the magnetosphere. The ring current was determined from the Voyager data [174]. However, the computations carried out with this model differed from the measurements carried out by Cassini during its first pass around Saturn in the Saturn orbit insertion (SOI). To satisfactorily describe the magnetic field measurements (especially in the external magnetosphere), a global model of the magnetosphere must include all three major current systems: the ring current, the magnetopause currents, and the current system of the magnetotail, and allow the parameters to vary with time. Computations in the framework of the paraboloid model were in good agreement with observations in the SOI orbit [159].

In 1980, Voyager for the first time detected kilometric emission from Saturn. Later, this emission was detected by Ulysses and Cassini, its origin being attributed to a cyclotron maser instability [149]. The period of pulses turned out to be close to that of the planet rotation and the emission intensity correlated with the dynamic pressure of the solar wind. Intense bursts of radioemission occurred when compression zones in the solar wind were approaching Saturn [175]. Apparently, the radio waves are excited as electrons lose energy on auroral field lines.

The intensity of the radio emission of Saturn is second only to the emission of Jupiter. The emission fills the frequency range from several kHz to 1.3 MHz and corresponds to the Saturn dipole magnetic moment 0.215 G R_p^3. A fine structure can be discerned in the dynamic spectrum of saturnian kilometric emissions. The kilometric emission ceases when the Saturn magnetosphere becomes enveloped by the Jupiter magnetotail [149]. The synchrotron emission of Saturn is very weak.

The sources of the kilometric radio emission and UV polar auroras of Saturn are mainly located in the dawn–day sector of field lines connected to the auroral region. The Kelvin–Helmholtz instability at the dawn magnetopause [176] or outflowing field-aligned current at the dawn side of the ionospheric boundary of the region of open field lines [177] have been proposed as mechanisms providing the necessary acceleration to electrons. It was assumed in both models that the velocity shear between the partly corotating plasma inside the magnetosphere and the compressed plasma of the magnetosheath flowing over it plays a dominant role in the process leading to electron precipitation [178]. The plasma speed in the magnetosheath depends on the solar wind velocity and the local time along the magnetopause.

An explanation of the observed 1% variation of the period of Saturn's kilometric emission is proposed in [178]. Because this emission is strictly controlled by the solar wind, it is assumed that variations of solar wind characteristics, especially the velocity, in Saturn's orbit may lead to a systematic shift of auroral sources of radio emission in time and to the modification of the apparent period of radio emission. The period of high-latitude auroral kilometric radio emission was used to determine the Saturn rotation period: 10 h 39.4 min.

In the near future, Cassini will continue to orbit Saturn and explore the planet and its rings and moons. The launch of the Probes research mission to Saturn, with the goal of studying its atmosphere, is scheduled for 2015. It was expected that the Tandem mission aimed at exploring Saturn's moons Titan and Enceladus would start orbiting Saturn around 2030. But in the framework of the Cosmic Vision program (2015–2025) of the European Space Agency, the choice between two missions, Laplace to Jupiter and Tandem to Saturn, was resolved in February 2009 in favor of the mission to Jupiter, which is scheduled for 2020.

6. Uranus's magnetosphere

Uranus is located at 19.18 AU from the Sun. Its mass exceeds the Earth's mass by a factor of 14, its density is 1.25 g cm^{-3}, and its radius is $R_U = 25{,}559$ km. The rotation period of Uranus depends on the latitude: it is 16.2 h at 33° and 14 h at 70° [36]. Uranus completes a revolution around the Sun in 84 Earth years. Uranus's rotation axis lies nearly in its orbital plane (it is tilted from the normal to the orbital plane by 97.9°) and is perpendicular to the direction of the planet orbital motion. The planet orbital plane practically coincides with the ecliptic plane. Uranus has moons, and a system of nine very narrow and dense rings surrounds the planet. The rings and moons of Uranus separated from it by up to 600,000 km are all in the plane nearly perpendicular to the ecliptic. The orbits of the more distant moons are oriented chaotically.

Uranus consist of three layers. The center hosts a core composed of metals, silicates, ammonia ice (NH_3), and methane (CH_4) and extends to about 0.3 of the planet radius. The mantle above it is composed of a mixture of water (H_2O) and ammonia–methane ices. The gaseous shell above the mantle measures approximately 0.3 of the planet radius. It is composed of hydrogen (85%), helium (12%), and methane (2.3%). Uranus, in contrast to other giant planets, emits less heat than it absorbs.

The two Voyager spacecraft were launched in 1977 with the goal of exploring the giant planets Jupiter and Saturn. Voyager 1 explored Jupiter in 1979 and then Saturn in 1980. It then left the Solar System, the heliosphere, moving in the direction the Sun moves with respect to the nearest stars. The directions of the outward motion of Pioneer 10 and Voyager 1 from the Sun are nearly opposite. The goals of the mission included the exploration of the upper distance limit at which the influence of the solar wind magnetic field and its radial velocity are still significant.

Voyager 2 flew around Jupiter in 1979 and around Saturn in 1981. Next it approached Uranus on 24 January 1986 and was closest to Neptune on 25 August 1989. On 30 August 2007, Voyager 2 left the Solar System. Both Voyagers will continue to study the sources of UV emission from stars. Their detectors of fields and particles are determining the boundary between the region where the influence of the Sun is essential and the interstellar medium. It is expected that the connection to the spacecraft will be in operation as long as their power supplies, which work on radioactive isotopes, will allow.

Thus, only a single spacecraft has been in the vicinity of Uranus thus far. On 24 January 1986, Voyager 2 was closest to Uranus, at the distance 107,000 km. At that time, the southern pole and the planet rotation axis were directed toward the Sun. Based on measurements from Voyager 2, the Uranus magnetic field was determined. The magnitude of the Uranus magnetic dipole is approximately 50 times larger than the Earth's. The contribution from the quadrupole term is comparable to the dipole one on the planet surface. It is only for Neptune that the quadrupole term makes an even larger contribution [179]. The authors of [180] were led to infer that magnetic moments of orders higher than the octupole can be significant only when the nondipole term in the planet magnetic field is large, which is true of the magnetic fields of Uranus and Neptune.

According to the Voyager data, the magnetic moment of the Uranus dipole, as distinct from those of Mercury, the Earth, Jupiter, and Saturn, is tilted at a large angle (59°) from the planet rotation axis and shifted toward the north pole by 8000 km [36]. As a result, the Uranus magnetosphere exhibits features related to the mutual location of the rotation and magnetic dipole axes. A bow shock is formed ahead of the Uranus magnetosphere, while an elongated magnetotail also exists. For Uranus, $R_1 = 25R_U$, and the distance to the bow shock is $33R_U$. There is some evidence in favor of the magnetospheric dynamics similar to the Earth's substorms [181, 182].

7. Neptune's magnetosphere

The Neptune mass exceeds the Earth mass by a factor of 17. Neptune's separation from the Sun is 30.02 AU, and its equatorial radius is $R_N = 24{,}764$ km. It is the smallest among the giant planets of the Solar System. Neptune completes a rotation around its axis in 16.1 h [179] and one revolution around the Sun in 165 years. The planet orbital plane is inclined at 1.8° to the ecliptic plane. The inclination between the equatorial and orbital planes is 29.6° (23° for Earth).

The atmosphere of Neptune, similarly to the other giant planets, comprises mainly hydrogen, with 15% helium and 1% methane. Owing to the presence of methane in the atmosphere, Neptune, like Uranus, has a blue hue: methane absorbs longer wavelengths of the solar spectrum and scatters blue and green light. It is assumed that an ocean of water saturated with various ions underlies the Neptune atmosphere. A significant amount of methane is contained deeper, in the icy mantle of the planet, where a mixture of water, methane, and ammonia can form solid ice. The hot icy mantle constitutes 70% of the planet mass, with the core making up about 25%. The Neptune core is composed of oxides of silicon, magnesium, iron and its derivatives, and rock. It is supposed that the pressure in the Neptune center amounts to 7 Mbar, and the temperature to $\sim$ 7000 K. The heat flux from its interior is almost three times larger than solar irradiation [36].

Twelve years after its launch, Voyager 2 reached the closest distance, 4950 km, to Neptune's cloud layer on 24–25 August 1989, and 5 years later it passed Neptune's moon Triton at the distance 40,000 km; Triton was the last space body explored by this spacecraft. In total, Voyager 2 explored Neptune from June to October 1989. It was found that the wind velocity in the Neptune atmosphere reaches 400–700 m s^{-1}. The rings of Neptune turned out to resemble those of Uranus, although the total surface area for Neptune is 100 times smaller. Neptune has numerous moons, the largest being Triton, roughly the size of the Moon. It is the only large moon in the Solar System orbiting its planet in the direction opposite to that of the planet rotation. This has allowed arguing that Neptune captured Triton during its motion in space.

The Neptune magnetic field is twice as weak as that of Uranus. Like Uranus, Neptune has a large nondipole component [183]. The contribution of the quadrupole moment to the magnetic field at the surface of Neptune is the largest among the planets of the Solar System [179].

The complex magnetic fields of Uranus and Neptune can be approximated fairly well by a dipole field shifted from the center and tilted from the rotation axis [184]. The magnetic dipole moment of Neptune exceeds that of the Earth by approximately a factor of 27. The angle between the dipole axis and the rotation axis is 47°. The dipole center is shifted to the southern hemisphere. Accordingly, the magnitude of the magnetic field at the southern magnetic pole is 10 times larger than at the northern one. The Neptune magnetic moment points to the north, similarly to Jupiter and Saturn, and opposite to the arrangement on the Earth.

The dipole representation is plausible only at distances greater than several planet radii. Close to the planet, the magnetic field can be expanded into a series in spherical harmonics with the accuracy increasing with the number of terms retained [180]. Because Voyager approached Neptune very closely (to the distance $1.18R_N$), it became possible to determine higher terms in the expansion of the Neptune internal field [180, 183].

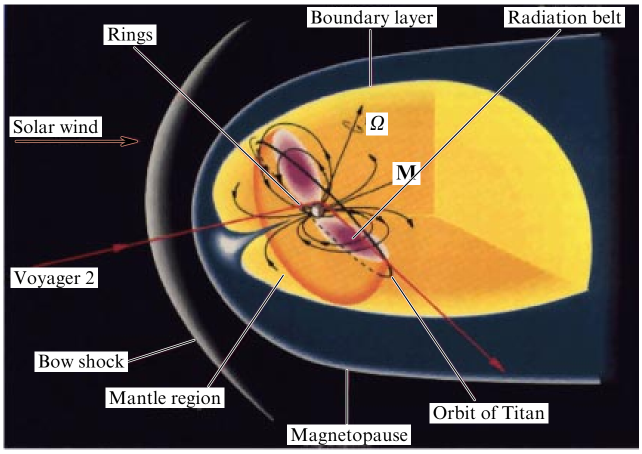

Figure 11. The Neptune magnetosphere. Courtesy of the Johns Hopkins University, USA (http://sd-www.jhuapl.edu/VOYAGER/neptune_gif.html). The schematic shows the solar wind, bow shock, magnetopause, boundary layer, mantle region, rings, radiation belt, the orbit of Titan, and the orbit of the Voyager spacecraft; Ω is the rotation axis and $\mathbf{M}$ is the planet dipole magnetic moment.

The magnetosphere of Neptune resembles that of Uranus. It is of medium size but still considerably larger than the Earth's magnetosphere. The relative sizes of the bow shock, magnetopause, and magnetotail are similar to those for the Earth. The distance to the magnetopause subsolar point R_1 is $26R_N$ for Neptune on the mean, and to the bow shock, $34R_N$ [179]. However, the structure of the Neptune magnetosphere is unique because it is defined by a particular geometry of the rotation and dipole axes. The Neptune magnetosphere is schematically displayed in Fig. 11. The Voyager spacecraft crossed the Neptune magnetosphere in August 1989 through the cusp [185] and stayed there for 38 h. During its passage, the magnetosphere remained quiet, no dynamical phenomena were recorded, and the southern magnetic pole was pointing toward the Sun.

The polar auroras on Neptune are fairly weak, as are the radio emissions. Because of the complex structure of the Neptune magnetic field, the polar auroras are a rather involved process, occurring over vast planetary regions offset from the magnetic poles.

8. Conclusions

This work presents a review of magnetospheres of planets in the Solar System that have an intrinsic magnetic field. A planet magnetic field serves as an obstacle to the impinging solar wind. A cavity, the magnetosphere, bound by a magnetopause carrying the currents screening the interplanetary medium from the magnetic field of magnetospheric sources, is formed around the planet. Besides the planet intrinsic magnetic field, these sources include large-scale current systems, the main ones of which are the magnetotail current system, the ring current, and the screening current at the magnetopause. It has been demonstrated that for all planets from Mercury to Saturn, interaction with the solar wind and its magnetic field is essential.

Sharing general properties, each magnetosphere shows its individual features governed by the planet parameters and location in the Solar System. The magnetosphere of Mercury is the most compact because of a relatively weak intrinsic magnetic field. Because of its proximity to the Sun, a marked role is played by the magnetic field of the solar wind. The Jupiter magnetosphere is the largest in the Solar System. Owing to fast rotation and the persistent source of plasma — the volcanic activity of Jupiter's moon Io, the magnetosphere is characterized by a powerful magnetodisk with a magnetic field exceeding the planet magnetic field, which is the strongest in the Solar System, by more than a factor of two. On the Earth, polar auroras occur because of the reconnection process of magnetospheric and interplanetary magnetic fields. On Jupiter, the polar auroras are linked to field-aligned currents flowing out of the ionosphere and originating because of a violation of the rigid corotation of plasma by radial outward motion. The Saturn magnetosphere is intermediate between those of Jupiter and the Earth. Saturn is also a rapidly rotating planet, but it carries a weaker magnetic field and has less intense sources of magnetospheric plasma than Jupiter. Thus, although a magnetodisk termed the ring current is formed in the Saturn magnetosphere, it is smaller than for Jupiter. Polar auroras on Saturn are strongly affected by the interaction with the solar wind and its magnetic field. The magnetospheres of Uranus and Neptune have been less studied, their specific features determined by the mutual orientation of the rotation axis and planetary magnetic field.

Direct measurements carried out with the help of spacecraft and ground-based data play a key role in exploring magnetospheres of Solar System planets. Direct measurements are assisted by the development of theoretical views and the design of models describing the available measurements and predicting forthcoming ones. Research into the interaction of the solar wind with magnetospheres of the Solar System planets is leading to new discoveries in plasma physics and astrophysics and is also prompting new questions and unsolved problems. The list of such problems includes, specifically, the dynamics and stability of current sheets and shear flows in a magnetized plasma and some details of the functioning of magnetospheric cyclotron masers [186]. Up to now, the mechanisms of electron acceleration causing polar auroras on planets remain vague.

Mediated by the solar wind, active processes on the Sun influence the state of magnetospheres of Solar System planets, and in particular the Earth's environment and technological and biological on-ground systems. Therefore, methods of forecasting solar activity and magnetic storms invite further research. These tasks are especially relevant is planning future space missions.

Despite obvious successes in the theory of the dynamo, there still exist large uncertainty as regards the applicability of various dynamic models to magnetic fields of the Sun and planets [2]. It is possible that the mechanism of the magnetic field generation on the Earth and on Jupiter is analogous to the process of a dynamo excited by convection in the interiors of rapidly rotating small-mass stars [187]. Thus far, there is no full clarity as regards the source of motion in the Earth's core that generates the Earth's dynamo. Under such circumstances, the most general and robust results independent of the details determining dynamic equations [2] gain in significance.

Although the results of theoretical works [188, 189] demonstrated that in some models, the dynamo system may evolve to a state in which its magnetic energy experiences finite-amplitude oscillations, it remains to learn whether such models relying on the equations of magnetic hydrodynamics in a rotating medium can explain reversals of the magnetic field polarity in spherical geometries. The problem remains one of the most important to the dynamo theory [2].

Plasma motions in laboratory conditions, in the Solar System, and in the far regions of the Universe generate magnetic fields, but these same plasma motions may also lead to reconnection of these fields [3]. It is currently known that this process is relevant for magnetospheres of the Solar System planets that have an intrinsic magnetic field, from Mercury to Saturn. However, the question of the impact of reconnection beyond the limits of the Solar System calls for research. Especially challenging is the theoretical research of reconnection because it includes a wealth of nonlinear nonideal processes in complex topologies [3].

Notwithstanding the focus of this review on magnetospheres of planets of the Solar System, it is worth mentioning that exoplanets — planets orbiting other stars — were recently discovered. There even exist exoplanets rotating around pulsars. The year 1995 saw the discovery of the first three exoplanets, but the 2006 catalogue of nearest exoplanets (< 200 ps) [190] already listed 172 exoplanets with a relatively low mass (< 24 of the Jupiter mass) detected through the measurements of radial velocity (by the Doppler shift) and apparent passage over the disk of the central star. For the first time, a planet traveling across the star disk was observed in 1999. In January 2008, the number of exoplanets increased to 228, and continues to increase. In addition to observable systems supporting standard views on the formation of stars and planets, a system with massive planets traveling in large-eccentricity orbits close to the central star have been unexpectedly detected. By virtue of the selection method used in observations, the majority of exoplanets discovered using it have masses equal to several Jupiter masses. Gaseous giants separated by < 0.1 AU from the central star have been named 'hot Jupiters.' They perform a revolution around their stars in < 11 days. After some reconstruction of powerful ground-based radio telescopes, it will be possible in the future, with the assistance of special observational methods, to search for radio emission from exoplanets.

In analogy with the interaction of magnetic planets of the Solar System with the solar wind, it is assumed that there may exist exoplanets having a magnetic field and interacting with the wind of their central stars. In this way, magnetospheres of exoplanets may form. But they should be different from magnetospheres of the planets in the Solar System. The differences are suggested, in particular, by the proximity of hot Jupiters to their central stars. Close to the star, the speed of the stellar wind is small, but the density and pressure are high. Intense streams of fast particles and X-ray emission, and also the influence of tides and coronal mass ejections should be expected. Because the stellar wind has a sub-Alfvén velocity, the bow shock does not form before the magnetosphere [191]. When the magnetic field of the stellar wind is parallel to the planet magnetic dipole moment, the energy released on magnetic reconnection can reach $\sim 10^{27}$ erg s^{-1}. A powerful energy release to auroral zones of exoplanets may occur and result in a strong observed outflow of matter from the atmospheres [191].

Acknowledgments

This paper was supported by the grant 07-05-00529 from the Russian Foundation for Basic Research. The review relies on the results obtained jointly with colleagues from the Numerical Mathematics Laboratory of the Institute for Nuclear Physics, Moscow State University: I I Alexeev, V V Kalegaev, M S Blokhin, M S Grigoryan, and S Yu Bobrovnikov, and also with foreign colleagues S W H Cowley (Radio and Space Plasma Group, University of Leicester, United Kingdom), J A Slavin (Heliophysics Science Division, NASA Goddard Space Flight Center, Greenbelt, USA), C R Clauer (Virginia Polytechnic Institute and State University), and R Prange (LESIA, Observatoire de Paris, Meudon, France). The author thanks them all and expresses her heartfelt gratitude for the fruitful collaboration.

References

1. Petrukovich A A, Dmitriev A V, Struminskii A B, in *Plazmennaya Geliofizika* (Plasma Heliophysics) Vol. 2 (Eds L M Zelenyi, I S Veselovskii) (Moscow: Fizmatlit, 2008) p. 176
2. Moffatt H K *Magnetic Field Generation in Electrically Conducting Fluids* (Cambridge: Cambridge Univ. Press, 1978) [Translated into Russian (Moscow: Mir, 1980)]
3. Priest E, Forbes T *Magnetic Reconnection: MHD Theory and Applications* (Cambridge: Cambridge Univ. Press, 2000) [Translated into Russian (Moscow: Fizmatlit, 2005)]
4. Horning G, in *Magnetic Helicity in Space and Laboratory Plasmas* (Eds M Brown, R C Canfield, A A Pevtsov) (Washington, DC: Am. Geophys. Union, 2000)
5. Siscoe G L et al. *J. Geophys. Res.* **106** (A7) 13015 (2001)
6. Kadomtsev B B *Kollektivnye Yavleniya v Plazme* (???) 2nd ed. (Moscow: Nauka, 1988) [Translated into English, in *Reviews of Plasma Physics* Vol. 22 (Ed. V D Shafranov) (New York: Kluwer Acad./Plenum Publ., 2001) p. 1]
7. Zelenyi L M, Malova Kh V, in *Plazmennaya Geliofizika* (Plasma Heliophysics) Vol. 2 (Eds L M Zelenyi, I S Veselovskii) (Moscow: Fizmatlit, 2008) p. 490
8. Dungey J W *Philos. Mag.* **44** 725 (1953)
9. Dungey J W, in *Geophysique Extérieure. Geophysics: The Earth's Environment. Lectures Delivered at Les Houches, 1962 Session* (Eds C DeWitt, J Hieblot, A Lebeau) (New York: Gordon and Breach, 1963) [Translated into Russian (Moscow: Mir, 1964)]
10. Crooker N U *J. Geophys. Res.* **84** (A3) 951 (1979)
11. Heppner J P, Maynard N C *J. Geophys. Res.* **92** (A3) 4467 (1987)
12. Cowley S W H *J. Geomagn. Geoelect.* **38** 1223 (1986)
13. Paschmann G et al. *J. Geophys. Res.* **91** (A10) 11099 (1986)
14. Paschmann G *Geophys. Res. Lett.* **35** L19109 (2008)
15. Gosling J T et al. *J. Geophys. Res.* **96** (A8) 14097 (1991)
16. Onsager T G et al. *J. Geophys. Res.* **106** (A11) 25467 (2001)
17. Mozer F S *J. Geophys. Res.* **110** A12222 (2005)
18. Vaivads A, Retinò A, André M *Space Sci. Rev.* **122** 19 (2006)
19. Zelenyi L M, Perumyan V, Ashur-Abdala M *Tr. Fiz. Inst. Ross. Akad. Nauk* **227** 70 (2000)
20. Bulanov S V et al. *Tr. Fiz. Inst. Ross. Akad. Nauk* **227** 48 (2000)
21. Syrovatsky S I *Tr. Fiz. Inst. Akad. Nauk SSSR* **74** 3 (1974)
22. Somov B V, Syrovatsky S I *Tr. Fiz. Inst. Akad. Nauk SSSR* **74** 14 (1974)
23. Somov B V *Kosmicheskaya Elektrodinamika i Fizika Solntsa* (Cosmic Electrodynamics and Solar Physics) (Moscow: Izd. MGU, 1993)
24. Vainshtein S I, Bykov A M, Toptygin I N *Turbulentnost', Tokovye Sloi i Udarnye Volny v Kosmicheskoi Plazme* (Turbulence, Current Sheets, and Shocks in Cosmic Plasma) (Moscow: Nauka, 1989) [Translated into English (Langhorne, Pa.: Gordon and Breach Sci. Publ., 1993)]
25. Petschek H E, in *The Physics of Solar Flares: Proc. of the AAS-NASA Symp., 1963* (Ed. W N Hess) (Washington, DC: Natl. Aeronautics and Space Administration, Science and Technical Information Division, 1964) p. 425
26. Priest E R, Titov V S *Philos. Trans. R. Soc. London A* **354** 2951 (1996)
27. Belenkaya E S *J. Geophys. Res.* **103** (A11) 26487 (1998)
28. Belenkaya E S *J. Atmos. Sol. Terr. Phys.* **60** 1343 (1998)
29. Pritchett P L, Coroniti F V *J. Geophys. Res.* **109** A01220 (2004)
30. Dungey J W *Phys. Rev. Lett.* **6** 47 (1961)
31. Cowley S W H *Radio Sci.* **8** 903 (1973)
32. Green J M *J. Geophys. Res.* **93** 8583 (1988)
33. Escoubet C P, Schmidt R, Goldstein M L, in *The Cluster and Phoenix Missions* (Eds C P Escoubet, C T Russell, R Schmidt) (Dordrecht: Kluwer Acad., 1997) p. 11
34. Phan T D et al. *Phys. Rev. Lett.* **99** 255002 (2007)
35. He J-S et al. *J. Geophys. Res.* **113** A05205 (2008)
36. Surdin V G (Ed.-Comp.) *Astronomiya: Vek XXI* (Astronomy: XXI Century) (Fryazino: Vek 2, 2008)
37. Alekseev I I, Kalegaev V V, in *Plazmennaya Geliofizika* (Plasma Heliophysics) Vol. 2 (Eds L M Zelenyi, I S Veselovskii) (Moscow: Fizmatlit, 2008) p. 422
38. Russell C T *Planet. Space Sci.* **49** 1005 (2001)
39. Russell C T *Planet. Space Sci.* **51** 731 (2003)
40. Zelenyi L M et al. *Usp. Fiz. Nauk* **175** 643 (2005) [*Phys. Usp.* **48** 615 (2005)]
41. Savin S P, in *Plazmennaya Geliofizika* (Plasma Heliophysics) Vol. 1 (Eds L M Zelenyi, I S Veselovskii) (Moscow: Fizmatlit, 2008) p. 398
42. Kovtyukh A S, Panasyuk M I, in *Plazmennaya Geliofizika* (Plasma Heliophysics) (Eds L M Zelenyi, I S Veselovskii) (Moscow: Fizmatlit, 2008) p. 506
43. Sonnerup B U Ö et al. *J. Geophys. Res.* **86** 10049 (1981)
44. Etemadi A et al. *Planet. Space Sci.* **36** 471 (1988)
45. Alekseev I I, Belenkaya E S *Geomagn. Aeron.* **23** 75 (1983)
46. Alekseev I I, Belenkaya E S *Geomagn. Aeron.* **26** 725 (1989)
47. Belenkaya E S *J. Geophys. Res.* **98** (A4) 5941 (1993)
48. Russell C T, in *Physics of the Magnetopause* (Geophys. Monograph, Vol. 90, Eds P Song, B U Ö Sonnerup, M F Thomsen) (Washington, DC: Am. Geophys. Union, 1995) p. 81
49. Phan T-D, Paschmann G, Sonnerup B U Ö *J. Geophys. Res.* **101** (A4) 7817 (1996)
50. Russell C T, in *Critical Problems of Magnetospheric Physics: Proc. of the Symp., 11–13 May, 1972, Madrid, Spain* (Ed. E R Dyer) (Washington, DC: Natl. Acad. of Sci., 1972) p. 1
51. Kaymaz Z et al. *J. Geophys. Res.* **101** (A6) 13321 (1996)
52. Alekseev I I *Geomagn. Aeron.* **18** 656 (1978)
53. Slavin J A et al. *J. Geophys. Res.* **90** (A11) 10875 (1985)
54. Alexeev I I et al. *J. Geophys. Res.* **101** (A4) 7737 (1996)
55. Alexeev I I, Feldstein Ya I *J. Atmos. Sol. Terr. Phys.* **63** 431 (2001)
56. Alexeev I I, Belenkaya E S, Clauer C R (Jr.) *J. Geophys. Res.* **105** (A9) 21119 (2000)
57. Feldstein Y I et al. *J. Geophys. Res.* **110** A11214 (2005)
58. Mead G D, Fairfield D H *J. Geophys. Res.* **80** 523 (1975)
59. Olson W P, Pfitzer K A *J. Geophys. Res.* **87** (A8) 5943 (1982)
60. Tsyganenko N A *Planet. Space Sci.* **35** 1347 (1987)
61. Tsyganenko N A *Planet. Space Sci.* **37** 5 (1989)
62. Hilmer R V, Voigt G-H *J. Geophys. Res.* **100** (A4) 5613 (1995)
63. Tsyganenko N A *J. Geophys. Res.* **100** (A4) 5599 (1995)
64. Maltsev Y P, Ostapenko A A *Geomagn. Aeron.* **41** 761 (2001) [*Geomagn. Aeron.* **41** 726 (2001)]
65. Tsyganenko N A *J. Geophys. Res.* **107** (A8) 1176 (2002)
66. Kuznetsov V D, in *Plazmennaya Geliofizika* (Plasma Heliophysics) Vol. 1 (Eds L M Zelenyi, I S Veselovskii) (Moscow: Fizmatlit, 2008) p. 81
67. Panasyuk M I et al. (Solar Extreme Events in 2003 Collab. (SEE-2003)) "Magnitnye buri v oktyabre 2003 g." *Kosmich. Issled.* **42** 509 (2004) ["Magnetic storms in October 2003" *Cosmic Res.* **42** 489 (2004)]
68. Alexeev I I, Feldstein Ya I *J. Atmos. Sol. Terr. Phys.* **63** 431 (2001)
69. Russell C T, Luhmann J G, Lu G *J. Geophys. Res.* **106** (A9) 18495 (2001)
70. Janhunen P et al. *Space Sci. Rev.* **122** 89 (2006)
71. Kozelov B V, in *Plazmennaya Geliofizika* (Plasma Heliophysics) Vol. 1 (Eds L M Zelenyi, I S Veselovskii) (Moscow: Fizmatlit, 2008) p. 569
72. Angelopoulos V et al. *Science* **321** 931 (2008)
73. Mauk B H, Anderson B J, Thorne R M, Preprint SPR-05-02 (Laurel, MD: Space Phys. Group, The Johns Hopkins Univ. Applied Phys. Lab., 2002)
74. Clauer C R et al. *J. Geophys. Res.* **106** (A11) 25695 (2001)
75. Russell C T et al. *Geophys. Res. Lett.* **19** 1227 (1992)

76. Ohtani S, Kokubun S, Russell C T *J. Geophys. Res.* **97** (A3) 3129 (1992)
77. Ginzburg V L *O Fizike i Astrofizike* (The Physics of a Lifetime) 3rd ed. (Moscow: Byuro Kvantum, 1995) [Translated into English (Berlin: Springer, 2001)]
78. Turyshev S G *Usp. Fiz. Nauk* **179** 3 (2009) [*Phys. Usp.* **52** 1 (2009)]
79. Giampieri G, Balogh A *Planet. Space Sci.* **49** 1637 (2001)
80. Ness N F et al. *J. Geophys. Res.* **80** 2708 (1975)
81. Anderson B J et al. *Science* **321** 82 (2008)
82. Siscoe G, Christopher L *Geophys. Res. Lett.* **2** 158 (1975)
83. Ogilvie K W et al. *J. Geophys. Res.* **82** 1807 (1977)
84. Wurz P, Blomberg L *Planet. Space Sci.* **49** 1643 (2001)
85. Boardsen S A, Slavin J A *Geophys. Res. Lett.* **34** L22106 (2007)
86. Slavin J A et al. *Science* **321** 85 (2008)
87. ZurbuchenT H et al. *Science* **321** 90 (2008)
88. Slavin J A, Holzer R E *J. Geophys. Res.* **86** (A13) 11401 (1981)
89. Slavin J A, Holzer R E *Phys. Earth Planet. Inter.* **20** 231 (1979)
90. Slavin J A *Adv. Space Res.* **33** 1859 (2004)
91. Slavin J A, Holzer R E *J. Geophys. Res.* **84** (A5) 2076 (1979)
92. Glassmeier K-H et al. *Space Sci. Rev.* **132** 511 (2007)
93. Shue J-H et al. *J. Geophys. Res.* **103** (A8) 17691 (1998)
94. Grard R *Planet. Space Sci.* **45** (1) 67 (1997)
95. Ness N F, in *Solar System Plasma Physics* Vol. 2 (Eds E N Parker, C F Kennel, L J Lanzerotti) (Amsterdam: North-Holland, 1979) p. 183
96. Alexeev I I et al. *J. Geophys. Res.* **113** A12210 (2008)
97. Sarantos M et al. *Planet. Space Sci.* **49** 1629 (2001)
98. Toffoletto F R, Hill T W *J. Geophys. Res.* **98** (A2) 1339 (1993)
99. Kabin K et al. *Icarus* **143** 397 (2000)
100. Ip W-H, Kopp A *J. Geophys. Res.* **107** (A11) 1348 (2002)
101. Kallio E, Janhunen P *Geophys. Res. Lett.* **30** 1877 (2003)
102. Kallio E, Janhunen P *Ann. Geophys.* **21** 2133 (2003)
103. Trávníček P, Hellinger P, Schriver D *Geophys. Res. Lett.* **34** L05104 (2007)
104. Lukyanov A V et al. *Planet. Space Sci.* **49** 1677 (2001)
105. Engle I M *Planet. Space Sci.* **45** 127 (1997)
106. Beard D B *J. Geophys. Res.* **84** (A5) 2118 (1979)
107. Luhmann J G, Russell C T, Tsyganenko N A *J. Geophys. Res.* **103** (A5) 9113 (1998)
108. Elsasser W M *J. Geophys. Res.* **61** 340 (1956)
109. Hill T W, Pontius D H (Jr.) *J. Geophys. Res.* **103** (E9) 19879 (1998)
110. Bunce E J, Cowley S W H *Planet. Space Sci.* **49** 261 (2001)
111. Connerney J E P, Acuña M H, Ness N F *J. Geophys. Res.* **86** (A10) 8370 (1981)
112. Belenkaya E S *Planet. Space Sci.* **52** 499 (2004)
113. Ness N F et al. *Science* **204** 982 (1979)
114. Ness N F et al. *Science* **206** 966 (1979)
115. Phillips J L et al. *Planet. Space Sci.* **41** 877 (1993)
116. Staines K et al. *Planet. Space Sci.* **41** 931 (1993)
117. Cowley S W H et al. *Planet. Space Sci.* **41** 987 (1993)
118. Cowley S W H et al. *J. Geophys. Res.* **101** (A7) 15197 (1996)
119. Goertz C K et al. *J. Geophys. Res.* **81** 3393 (1976)
120. Cowley S W H, Deason A J, Bunce E J *Ann. Geophys.* **26** 4051 (2008)
121. Rego D et al. *Nature* **399** 121 (1999)
122. Clarke J T "Satellite Footprints Seen in Jupiter Aurora", Space Telescope Science Institute Press Release STScI-PRC00-38 (Baltimore, MD, December 14) (2000)
123. Hill T W *J. Geophys. Res.* **106** (A5) 8101 (2001)
124. Laxton N F et al. *Planet. Space Sci.* **47** 205 (1999)
125. Belenkaya E C *Geomagn. Aeron.* **43** (2) 174 (2003)
126. Alexeev I I, Belenkaya E S *Ann. Geophys.* **23** 809 (2005)
127. Alekseev I I, Belenkaya E S, in *Plazmennaya Geliofizika* (Plasma Heliophysics) Vol. 2 (Eds L M Zelenyi, I S Veselovskii) (Moscow: Fizmatlit, 2008) p. 61
128. Goldstein M L, Lepping R P, Sittler E C (Jr.) *J. Geophys. Res.* **90** (A9) 8223 (1985)
129. Goldstein M L, Lepping R P, Sittler E C (Jr.) *J. Geophys. Res.* **91** (A6) 7133 (1986)
130. Hill T W, Dessler A J, Michel F C *Geophys. Res. Lett.* **1** 3 (1974)
131. Barish F D, Smith R A *Geophys. Res. Lett.* **2** 269 (1975)
132. Smith E J et al. *Science* **188** 451 (1975)
133. Beard D B, Jackson D J *J. Geophys. Res.* **81** 3399 (1976)
134. Goertz C K, in *Jupiter, the Giant Planet* (Ed. T Gehrels) (Tucson, AZ: Univ. of Arizona Press, 1976) p. 23
135. Goertz C K *J. Geophys. Res.* **81** 3368 (1976)
136. Goertz C K *Space Sci. Rev.* **23** 319 (1979)
137. Engle I M, Beard D B *J. Geophys. Res.* **85** (A2) 579 (1980)
138. Acuña M H, Behannon K W, Connerney J E P, in *Physics of the Jovian Magnetosphere* (Ed. A J Dessler) (New York: Cambridge Univ. Press, 1983) p. 1
139. Connerney J E P *J. Geophys. Res.* **86** (A9) 7796 (1981)
140. Connerney J E P et al. *J. Geophys. Res.* **103** (A6) 11929 (1998)
141. Khurana K K *J. Geophys. Res.* **102** (A6) 11295 (1997)
142. Connerney J E P *J. Geophys. Res.* **98** (E10)18659 (1993)
143. Khurana K K et al., in *Jupiter: The Planet, Satellites, and Magnetosphere* (Eds F Bagenal, T E Dowling, W B McKinnon) (Cambridge: Cambridge Univ. Press, 2004) p. 593
144. Kivelson M G, Southwood D J *Planet. Space Sci.* **51** 891 (2003)
145. Walker R J, Ogino T, Kivelson M G *Planet. Space Sci.* **49** 237 (2001)
146. Zarka P, Kurth W S *Space Sci. Rev.* **116** 371 (2005)
147. Carr T D, Desch M D, Alexander J K, in *Physics of the Jovian Magnetosphere* (Ed. A J Dessler) (New York: Cambridge Univ. Press, 1983) p. 226
148. Burke B F, Franklin K L *J. Geophys. Res.* **60** 213 (1955)
149. Roberts J A *Usp. Fiz. Nauk* **83** 503 (1964); *Planet. Space Sci.* **11** 221 (1963)
150. Ryabov B P, Gerasimova N N *Dekametrovoe Sporadicheskoe Radioizluchenie Yupitera* (Decameter Sporadic Emission of Jupiter) (Kiev: Naukova Dumka, 1990)
151. Gurnett D A et al. *Nature* **415** 985 (2002)
152. Rucker H O et al. *Astrophys. Space Sci.* **277** 325 (2001)
153. Zaitsev V V, Shaposhnikov V E, Rucker H O *Adv. Space Res.* **36** 2106 (2005)
154. Zaitsev V V, Shaposhnikov V E, Rucker H O *Astron. Astrophys.* **454** 669 (2006)
155. Fortov V E et al. *Usp. Fiz. Nauk* **166** 391 (1996) [*Phys. Usp.* **39** 363 (1996)]
156. Smith E J et al. *J. Geophys. Res.* **85** (A11) 5655 (1980)
157. Sittler E C (Jr.), Ogilvie K W, Scudder J D *J. Geophys. Res.* **88** (A11) 8847 (1983)
158. Belenkaya E S et al. *Ann. Geophys.* **24** 1145 (2006)
159. Alexeev I I et al. *Geophys. Res. Lett.* **33** L08101 (2006)
160. Cowley S W H, Bunce E J *Ann. Geophys.* **21** 1691 (2003)
161. Badman S V et al. *J. Geophys. Res.* **110** A11216 (2005)
162. Clarke J T et al. *Nature* **433** 717 (2005)
163. Bunce E J et al. *Adv. Space Res.* **38** 806 (2006)
164. Belenkaya E S, Cowley S W H, Alexeev I I *Ann. Geophys.* **24** 1649 (2006)
165. Belenkaya E S et al. *Ann. Geophys.* **25** 1215 (2007)
166. Belenkaya E S et al. *Ann. Geophys.* **26** 159 (2008)
167. Prangé R et al. *Nature* **432** 78 (2004)
168. Cowley S W H, Bunce E J, Prangé R *Ann. Geophys.* **22** 1379 (2004)
169. Jackman C M et al. *J. Geophys. Res.* **109** A11203 (2004)
170. Davis L (Jr.), Smith E J *J. Geophys. Res.* **95** (A9) 15257 (1990)
171. Connerney J E P, Acuña M H, Ness N F *J. Geophys. Res.* **88** 8779 (1983)
172. Bunce E J, Cowley S W H *Ann. Geophys.* **21** 661 (2003)
173. Maurice S, Engle I M *J. Geophys. Res.* **100** (A9) 17143 (1995)
174. Dougherty M K et al. *Science* **307** 1266 (2005)
175. Badman S V et al. *Ann. Geophys.* **26** 3641 (2008)
176. Galopeau P H M, Zarka P, Le Quéau D *J. Geophys. Res.* **100** (E12) 26397 (1995)
177. Talboys D L et al. *J. Geophys. Res.* **114** A06220 (2009)
178. Cecconi B, Zarka P *J. Geophys. Res.* **110** A12203 (2005)
179. Russell C T, Luhmann J G, in *Encyclopedia of Planetary Sciences* (Eds J H Shirley, R W Fairbridge) (New York: Chapman & Hall, 1997)
180. Ho C W, Huang T S, Gao S *J. Geophys. Res.* **102** (A11) 24393 (1997)
181. Mauk B H et al. *J. Geophys. Res.* **92** (A13) 15283 (1987)
182. Sittler E C (Jr.), Ogilvie K W, Selesnick R *J. Geophys. Res.* **92** (A13) 15263 (1987)
183. Connerney J E P, Acuña M H, Ness N F *J. Geophys. Res. Suppl.* **96** 19023 (1991)
184. Ness N F et al. *Science* **246** 1473 (1989)
185. Belcher J W et al. *Science* **246** 1478 (1989)
186. Zelenyi L M, in *Plazmennaya Geliofizika* (Plasma Heliophysics) Vol. 2 (Eds L M Zelenyi, I S Veselovskii) (Moscow: Fizmatlit, 2008) p. 11
187. Christensen U R, Holzwarth V, Reiners A *Nature* **457** 167 (2009)
188. Proctor M R E *Astron. Nachrichten* **298** 19 (1977)
189. Soward A M *Philos. Trans. R. Soc. London A* **275** 611 (1974)
190. Butler R P et al. *Astrophys. J.* **646** 505 (2006)
191. Ip W-H, Kopp A, Hu J-H *Astrophys. J.* **602** L53 (2004)